Chapter 3
Experimental Characterization of Peptide–Surface Interactions

Marion J. Limo, Carole C. Perry, A. A. Thyparambil, Yang Wei and Robert A. Latour

Abstract Interactions between peptides and proteins with material surfaces are fundamental to a broad range of applications in biotechnology and biomedical engineering. Many different methods have been developed to measure a range of properties that quantify these types of interactions. In this chapter, three of these methods are presented for the determination of thermodynamic parameters that characterize peptide adsorption behavior, each of which is based on a different type of measurement. These three methods are surface plasmon resonance spectroscopy (SPR; spectroscopic-based method), atomic force microscopy (AFM; force-based method), and isothermal titration calorimetry (ITC; thermal-based method). The fundamental principles underlying each of these methods are presented followed by examples of their application for the determination of thermodynamic properties for specific peptide/protein-surface systems. The SPR method is presented for the determination of the standard-state adsorption free energy from adsorption isotherms characterizing the amount of peptide adsorbed as a function of solution concentration. This method, however, is limited to materials that can be used to form nanoscale-thick films about 100 nm thick or less on a gold biosensor substrate. For materials that are not easily formed into thin films, thus not being conducive for use with SPR, an AFM method is presented that can be used with any macroscopically flat surface through the correlation of peptide desorption force measured by AFM with adsorption free energy measurements by SPR. The third approach, ITC, measures thermal energy changes on adsorption with the method being applicable to the interaction of peptides/proteins with particles suspended in solution. The combined set of methods provides the

M. J. Limo · C. C. Perry (✉)
Interdisciplinary Biomedical Research Centre, Department of Chemistry and Forensic Science, School of Science and Technology, Nottingham Trent University, Clifton Lane, Nottingham NG11 8NS, UK
e-mail: carole.perry@ntu.ac.uk

A. A. Thyparambil · Y. Wei · R. A. Latour
Department of Bioengineering, 501 Rhodes Engineering Research Center, Clemson University, Clemson, SC 29634, USA

M. R. Knecht and T. R. Walsh (eds.), *Bio-Inspired Nanotechnology*,
DOI: 10.1007/978-1-4614-9446-1_3,

means to quantitatively determine thermodynamic properties characterizing peptide and protein adsorption behavior for materials in either their bulk or particulate form, with important application to the broad range of technologies that involve contact between biological solutions and synthetic material surfaces.

3.1 Introduction

The interactions of proteins with material surfaces is of critical importance in many areas of biotechnology and biomedical engineering, including implant biocompatibility (Kasemo and Gold 1999; Bryers et al. 2012), tissue engineering and regenerative medicine (Garcia 2006; Mahmood et al. 2006; Gandavarapu et al. 2013), biosensors (Wisniewski et al. 2000; Geelhood et al. 2007), drug delivery systems (Liu and Webster 2010; Gref et al. 2012), enzyme-based technologies (Knowles 1991; Blankschien et al. 2013; Wu et al. 2013), and biodefense (Bramwell et al. 2005; Herr 2009). Proteins are, of course, made up of unique linear sequences of amino acids that form polypeptide chains, which constitute a protein's primary structure. These polypeptide chains then fold to form secondary, tertiary, and possibly quaternary levels of structure. The resulting geometric shape, dynamics, and surface chemistry of these hierarchical structures subsequently create bioactive sites that enable proteins to perform their designated functions, such as cell signaling, biosensing, biotransport, or biocatalysis. Due to the extreme complexity of proteins, it can be very difficult to quantitatively determine and understand the molecular-level interactions that occur in proteins when they come in contact with synthetic material surfaces, either through nonspecific or specific adsorption from solution, physical entrapment, or through direct covalent linkage. However, molecular-level insights into protein–surface interactions can be obtained by studying the interactions of small portions of a protein, i.e., short sequences of amino acids (or peptides), which can be isolated from a given protein once its structure has been determined. Furthermore, many peptides have substantial bioactivity themselves apart from being integrated within a larger protein structure, such that an understanding of their interactions with material surfaces is important in its own right.

Given the importance of the behavior of peptides when they come in contact with material surfaces, experimental methods are needed to quantitatively characterize peptide-surface interactions. Over the past few decades, several experimental techniques have been developed to study peptide adsorption behavior on material surfaces. These methods include atomic force microscopy (AFM), ellipsometry, isothermal titration calorimetry (ITC), optical waveguide lightmode spectroscopy (OWLS), quartz crystal microbalance (QCM), sum-frequency generation (SFG), and surface plasmon resonance spectroscopy (SPR). In this chapter, we focus on just three of these methods, which the authors have been applying and

further developing in their own laboratories to study the thermodynamics of peptide–surface interactions. These three methods are AFM, SPR, and ITC. The principles by which binding information is obtained for all three experimental approaches requires measurement of the 'force' of interaction (AFM), 'spectroscopic' measurement of interaction (SPR), and direct 'thermal' measurement of the thermodynamics of interaction (ITC). In all cases irrespective of the mode of measurement, thermodynamic data relating to the 'strength' of interaction can be obtained. In the subsequent sections of this chapter, details are presented on each of these three experimental methods along with an overview of methods used for analysis of the experimental data obtained by implementation of these methods. Examples are then provided to demonstrate how these techniques have been applied to characterize the behavior of a broad range of peptide–surface systems.

3.2 Surface Plasmon Resonance Spectroscopy

3.2.1 Surface Plasmons

Surface plasmons are guided electron oscillations confined to a thin layer of the interface between two materials with negative and positive real parts of permittivity (e.g., a metal–dielectric interface). The principle of SPR occurs when the incident light wave-vector component parallel to the interface matches the propagation constant of the surface plasmon (Pitarke et al. 2007).

This condition is only satisfied at distinct angles of incidence, appearing as a drop in the reflectivity of incident light from which the optical energy is dissipated into a guided electromagnetic wave along the interface (Homola et al. 1999). As the extent of energy transfer is sensitive to any coupling conditions close to the interface, SPR biosensing relies on the principle that changes in the local index of refraction near the dielectric sensing surface, which can be brought about by changes in solution concentration local to the sensor surface (e.g., from mass adsorption to the surface), will cause a shift in the angle of reflectivity, which can be sensed by a suitable detector. This serves as the basis for various SPR sensors used in either qualitative or quantitative mode to determine the molecular binding events or kinetics and affinity parameters of molecular interactions (Jung et al. 1999; Green et al. 2000; Zhang et al. 2003; Taylor et al. 2008; Chen and Ming 2012).

3.2.2 SPR Spectroscopy

The use of optical sensors based on SPR has become one of the most important tools in molecular interaction analysis in the past decade due to its real-time monitoring capability with high sensitivity (Chen and Ming 2012). For these reasons, SPR

spectroscopy has also been recognized as one of the most directly applicable methods to characterize adsorption/desorption behavior to determine kinetic and thermodynamic parameters, such as the rates of adsorption/desorption and adsorption free energies, respectively (Haruki et al. 1997; Loomans et al. 1997; Li and Husson 2006; Tamerler et al. 2006). This technique is particularly well suited for use with Au-alkanethiol self-assembled monolayers (SAMs) because of gold's ability to exhibit a strong plasmon resonance signal, and has been widely applied in recent years to study both peptide and protein adsorption behavior on these types of model surfaces (Silin et al. 1997; Vernekar and Latour 2005).

However, whereas SPR is a useful technique for measuring peptide-SAM surface interactions, its usefulness is limited to materials that can form high-quality uniform nanoscale-thick films (e.g., <100 nm) on a metallic surface that can be used to generate an SPR signal (Wei and Latour 2010). Many materials, including most polymers, ceramics, and inorganic glasses, are thus not readily suitable for use with SPR spectroscopy. Therefore, alternative methods are needed to characterize peptide–surface interactions for these types of materials.

3.3 Atomic Force Microscopy

Compared with SPR, AFM has also been widely applied to characterize biological molecular recognition processes because of its high force sensitivity and the capability of operating under different physiological conditions and on any material with a macroscopically flat surface (Lal and John 1994; Willemsen et al. 2000; Allison et al. 2002; Kidoaki and Matsuda 2002). However, the use of AFM for these applications can result in difficulties in interpreting molecular force data (e.g., adsorption behavior) for peptide–surface interactions due to the absence of a direct way to determine the actual number of interacting molecules for a corresponding force measurement (Blanchette et al. 2008). One approach to overcome this problem is to correlate AFM results for peptide–surface interactions using a standardized AFM methodology to thermodynamic measurements for the same systems obtained by another surface sensitivity technique, such as SPR spectroscopy (Wei and Latour 2010). This approach then enables the same probe tip density to be consistently used for the measurements even though the actual number of tethered chains is unknown.

3.4 Combined SPR and AFM Methods

It has been shown that desorption forces (F_{des}) obtained using a standardized AFM method correlate linearly with $\Delta G^{o}_{\mathrm{ads}}$ values measured from SPR for peptide–surface interactions under a range of different solvent conditions, including both

potassium phosphate buffer (PPB) and phosphate buffered saline (PBS) at pH 7.4 for salt concentrations below about 150 mM (Thyparambil et al. 2012; Wei et al. 2012). This combined set of approaches thus provide a means to directly determine ΔG^o_{ads} for peptide adsorption to surfaces that can be used with SPR, or to indirectly determine ΔG^o_{ads} for any macroscopically flat material surface that is not conducive to SPR by using this correlated AFM technique. In this section, we introduce the combined SPR and AFM methods that we have developed to characterize peptide adsorption behavior and show how they can be used to experimentally provide ΔG^o_{ads} values (by SPR) and effective ΔG^o_{ads} values (by AFM) for a wide variety of peptide–surface combinations using a relatively simple, straightforward adsorption system.

3.4.1 Surface Preparation and Characterization: Self-Assembled Monolayers on Gold and Material Surfaces Not Conducive to SPR

3.4.1.1 Surface Preparation

For both SPR and AFM studies, we have used alkanethiol SAM surfaces on gold with the structure of Au–S(CH2)11–Y, with Y representing functional groups contained in a wide range of organic polymers, such as: Y = OH, CH_3, OC_6H_5, NH_2, COOH, $NHCOCH_3$, $COOCH_3$, and EG_3OH (EG: ethylene glycol segment (–O–CH_2–CH_2–). We have also investigated material surfaces that are not conducive for SPR, including fused silica glass and quartz (Chemglass Life Sciences, Vineland, NJ), high-density polyethylene (HDPE) (MW = 125,000 Da, Sigma Chemical Co., St. Louis, MO), and poly(methyl-methacrylate) (PMMA) (MW=350,000 Da, Sigma Chemical Co., St. Louis, MO). HDPE and PMMA surfaces are spin-coated from dodecalin (0.5 % (w/w) at 1,500 rpm for 60 s) and chloroform solutions (1.5 % (w/w) at 1,000 rpm for 60 s), respectively, onto fused silica glass slides, although bulk material surfaces can also be used.

3.4.1.2 Surface Characterization

Surface characterization is an extremely important component of any adsorption study in order to obtain as much quantitative information as possible regarding the physical and chemical structure of the surface. For our studies, surface characterization was performed to determine the static air–water contact angle, atomic composition, film thickness, and surface roughness of the substrates used. For all the surfaces, the static air–water contact angle values were analyzed using a CAM 200 optical contact angle goniometer (KSV Instruments Inc., Monroe, CT) and the atomic compositions were verified via X-ray photoelectron spectroscopy

Table 3.1 Surface characterization: Atomic composition for each surface

Surface moiety	*C* (%)	*S* (%)	*N* (%)	*O* (%)
–OH	56.7 (0.8)	2.8 (0.6)	*	7.5 (0.2)
$–CH_3$	64.9 (0.7)	2.8 (0.2)	*	*
$–(EG)_3OH$	54.8 (0.3)	2.3 (0.1)	*	13.2 (0.6)
$–NH_2$	54.0 (0.9)	2.0 (0.2)	4.0 (0.3)	3.3 (0.3)
–COOH	47.6 (1.8)	1.6 (0.1)	*	7.6 (0.3)
$–OC_6H_5$	56.2 (0.9)	2.4 (0.2)	*	5.3 (0.9)
$–NHCOCH_3$	48.6 (0.6)	1.7 (0.1)	4.0 (0.1)	6.0 (0.7)
$–COOCH_3$	45.4 (4.3)	2.5 (0.2)	*	10.8 (0.6)
Fused Glass**	25.0 (2.0)	*	<1.0	49.0 (2.0)
Quartz (100)**	15.0 (2.0)	<1.0	<2.0	53 (1.0)
PMMA	76.0 (1.0)	*	*	24.0 (1.0)
HDPE	96.0 (3.0)	*	*	3.0 (3.0)

An asterisk (*) indicates negligible value for atomic composition data. (Mean ± 95 % confidence interval (C.I.), $N = 3$). Reprinted from Thyparambil et al. (2012) with permission

** Glass slide also contains Zn (<1 %), Al (<1 %) and Si (22.0 ± 1.0 %) while the quartz surface of specific orientation (100) contains Si (30.0 ± 3.0 %) in atomic composition by XPS (not shown). The presence of extra carbon composition is believed to be originating from surface contamination due to the exposure of samples to air after the cleaning procedure. These are the typical adventitious and unavoidable hydrocarbon impurities that adsorb spontaneously from ambient air onto the glass and quartz surfaces

(NESAC/BIO, University of Washington, Seattle, WA). Average surface roughness was analyzed using MFP-3D AFM (Asylum Research, Santa Barbara, CA) over an area of 5 × 5 μm. The film thicknesses of the SAMs and polymer films were characterized using a GES-5 variable angle spectroscopic ellipsometer (Sopra Inc., Palo Alto, CA). Tables 3.1 and 3.2 present results obtained for our surfaces by these characterization methods.

3.4.2 Host–Guest Peptide Model

The host–guest model peptides that we designed for our studies (synthesized by Biomatik, Wilmington, DE; characterized by analytical HPLC and mass spectral analysis with 98 % purity) have the amino acid sequence of TGTG-X-GTGT (for SPR studies) and TGTG-X-GTCT (for AFM studies) with zwitterionic end groups, where G, T, and C are glycine (–H side chain), threonine ($–CH(CH_3)OH$ side chain), and cysteine ($–CH_2SH$ side chain), respectively. *X* represents a "guest" amino acid residue, which can be any of the 20 naturally occurring amino acid types. This residue is placed in the middle of the peptide to represent the characteristics of a mid-chain amino acid in a protein by positioning it relatively far from the zwitterionic end groups of the peptide. The threonine (T) residues and the zwitterionic end groups were selected to enhance aqueous solubility and to provide additional molecular weight for SPR detection while the non-chiral glycine

Table 3.2 Surface characterization: Static water contact angle, film thickness, and surface roughness analyses for each surface

Surface moiety	Roughness (nm)	Contact angle (°)	Thickness (Å)
–OH	<0.5	16 (2)	13.0 (1.0)
$–CH_3$	<0.5	110 (3)	11.0 (1.0)
$–(EG)_3OH$	<0.5	32 (3)	19.0 (3.0)
$–NH_2$	<0.5	48 (2)	14.7 (2.5)
–COOH	<0.5	18 (1)	15.8 (2.0)
$–OC_6H_5$	<0.5	80 (4)	14.4 (4.0)
$–NHCOCH_3$	<0.5	48 (2)	17.0 (2.0)
$–COOCH_3$	<0.5	63 (2)	11.0 (4.8)
Fused glass	<10.0	23 (4)	**
Quartz (100)	<1.5	13 (3)	**
PMMA	<1.5	63 (3)	90 (10) in nm
HDPE	<8.0	97 (5)	100 (10) in nm

Mean ± 95 % confidence interval (C.I.), $N = 3$. Reprinted from Thyparambil et al. (2012) with permission

**Custom cut glass slides (0.375″ × 1.625″ × 0.0625″, Chemglass Life Sciences, NJ) and custom cut quartz (100) (0.375″ × 1.625″ × 0.0625″, MTI Corporation, Richmond, CA)

residues were selected to inhibit the formation of secondary structure, thus simplifying its adsorption behavior. The cysteine (C) residue was required for the AFM studies as the linker to connect our host–guest peptide sequences to the AFM probe tip (Wei and Latour 2010). Preliminary SPR studies that we have conducted using both of these peptide models have indicated that the TGTG-X-GTCT peptide can be used in AFM studies as an equivalent system for comparison with the TGTG-X-GTGT peptide model used by SPR (Wei and Latour 2010; Thyparambil et al. 2012).

3.4.3 Solvent Environment

All peptide–surface interactions were investigated either in phosphate-buffered saline (PBS; Fisher Scientific, Fair Lawn, NJ) or in 10 mM potassium phosphate buffer (PPB; Sigma Chemical Co., St. Louis, MO) at a bulk solution pH of 7.4. PBS is a complex mixture of salts in aqueous solution (140 mM sodium chloride, 10 mM sodium phosphate, 2.7 mM potassium chloride, and 1.8 mM potassium phosphate). The PPB buffer used here is a homogenous simple minimum salt solution that contains only 10 mM phosphate salts of potassium (Fisher Scientific, Fair Lawn, NJ) as needed for pH control. All buffer solutions were filtered and degassed prior to use.

3.4.4 Determination of ΔG^o_{ads} by SPR Spectroscopy

To determine ΔG^o_{ads} accurately for peptide adsorption using SPR, two key issues must be addressed: the need to account for (i) "bulk-shift" effects and (ii) the influence of solute–solute interactions on the surface.

Because SPR measures the refractive index change of the medium within a distance of about 300 nm of the plasmon-producing surface, it is sensitive to both the molecules adsorbed at the interface and the molecules suspended in the medium within this 300 nm distance (de Mol and Fischer 2010). This latter contribution, known as the "bulk effect," introduces a component into the SPR signal that is linearly proportional to the mass concentration of the analyte in the solution. Therefore, to determine the amount of SPR signal that is due to the adsorption process, the bulk-shift contribution must be subtracted from the raw SPR signal that is obtained during the adsorption experiment (Wei and Latour 2008).

Peptide–peptide interactions present another problem that can greatly skew the shape of the adsorption isotherm and result in erroneous calculated values of ΔG^o_{ads}. ΔG^o_{ads} is determined from the equilibrium constant, K_{eq}, of a reversible adsorption process, which represents the partition coefficient for the concentration of the solute on a surface versus its concentration in bulk solution. Ideally, the value of K_{eq} could be determined as the initial slope in the linear region of the adsorption isotherm, which represents infinite dilution conditions, in order to minimize effects from solute–solute interactions at the surface (Charles and Abraham 2003). Unfortunately, this requires the measurement of adsorption events for solution concentrations that typically extend well below the detection limit of currently available commercial SPR instruments. To get around this problem, an adsorption model, such as the Langmuir model, is generally used to calculate ΔG^o_{ads} on the basis of the overall shape of the isotherm. This, however, creates additional complications because solute–solute interactions may occur on the surface as the surface sites become filled, which can substantially influence the shape of the isotherm and invalidate the application of the Langmuir adsorption model. If the Langmuir model is still used despite the occurrence of solute–solute interactions, then substantial error will be introduced into the calculated value of ΔG^o_{ads} (Wei and Latour 2008).

To address both of these problems, we conduct peptide adsorption experiments with SPR using a Biacore X SPR spectrometer (Biacore, Inc., Piscataway, NJ) in either PPB or PBS, pH 7.4, using the following methods (Wei and Latour 2008, 2009). Briefly, SPR sensorgrams for peptide adsorption are recorded in the form of resonance units [RU; 1 RU = 1.0 pg/mm^2 (Stenberg et al. 1991)] as a function of time for six independent runs of varied peptide concentrations over each SAM surface at 25 °C. The data obtained are then used to generate isotherm curves by plotting the raw SPR signal (i.e., the signal from both surface adsorption and solution bulk-shift effects) as a function of peptide solution concentration.

The equation that we use for the determination of ΔG^o_{ads} from the adsorption isotherms was derived based on the chemical potential of the peptide in its adsorbed versus bulk solution state (Wei and Latour 2009). During an SPR experiment to measure the adsorption of a peptide to a surface, the overall change in the SPR signal (i.e., the raw SPR signal) reflects both of the excess amount of adsorbed peptide per unit area, q (measured in RU), and the bulk-shift response, which is linearly proportional to the concentration of the peptide in solution. This relationship can be expressed as:

$$\mathrm{SPR} = q + mC_b = \frac{QC_b}{C_b + C^o K^{-1}} + mC_b \tag{3.2}$$

where C_b (mol/L, M) is the concentration of the peptide in bulk solution, $C°$ is the peptide solution concentration under standard-state conditions (taken as 1.0 M), m (RU/M) is the proportionality constant between the bulk shift in the SPR response and the peptide molar concentration in the bulk solution, K (unitless) is the effective equilibrium constant for the peptide adsorption reaction, and Q (RU) is amount of peptide adsorbed at surface saturation. Each isotherm plot of the raw SPR response versus C_b is fit with Eq. (3.2) by nonlinear regression to solve for the parameters Q, K, and m using a nonlinear statistical analysis software program (e.g., SAS Institute, Cary, NC). However, it should be understood that the values of Q and K determined by this fit may be substantially influenced by peptide–peptide interactions on the surface. In order to measure peptide adsorption behavior with minimal influence from peptide–peptide interactions, we use the premise that peptide–peptide interactions are minimized at very low solution concentrations, but then influence the isotherm shape (and thus the values of Q and K) as the surface becomes crowded at higher values of C_b. The initial slope of the isotherm where C_b approaches zero should thus be minimally influenced by peptide–peptide interactions. Based on this principle, we have derived the relationship shown in Eq. (3.3), which enables ΔG^o_{ads} to be determined from an adsorption isotherm that is generated by SPR with minimal influence of peptide–peptide interactions. Readers are referred to our initial publication of this method for details on this derivation (Wei and Latour 2008), with the derivation basically involving the use of the fitted parameters (i.e., Q and K) to estimate the slope of the isotherm as Cb approaches zero. Accordingly, ΔG^o_{ads} (kcal/mol) is calculated from the parameters obtained from our raw SPR sensorgrams as:

$$\Delta G^o_{ads} = -RT\ln\left[\left(\frac{C_s}{C_b}\right)_{C_b \to 0}\right] = -RT\ln\left(\frac{QK}{\delta C^0} + 1\right) \tag{3.3}$$

where the theoretically defined parameter δ is the thickness of the adsorbed layer of the peptide (calculated to be about 1.2 nm), R (kcal/mol·K) is the ideal gas constant, and T (K) is the absolute temperature.

We have applied these methods to characterize the adsorption response of a large range of peptide-surface systems for the determination of ΔG^o_{ads}. Figure 3.1 shows

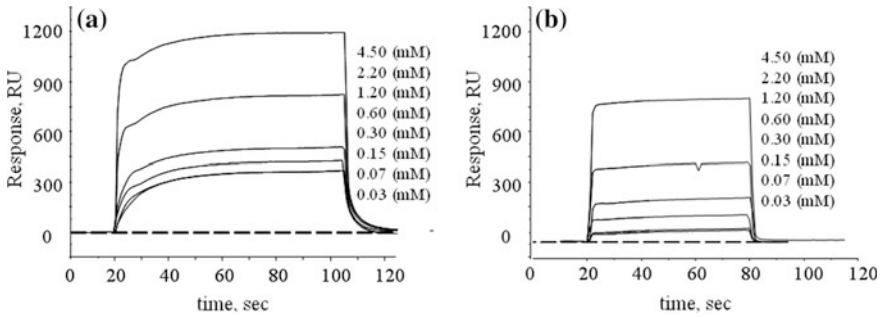

Fig. 3.1 Response curves (SPR signal (RU) versus time for TGTG-V-GTGT on **a** SAM-CH_3 and **b** SAM-OH surface (not all of the concentration curves are listed for clarity sake because some of the low concentration curves overlap one another and are thus not separately distinguishable). Reprinted from Thyparambil et al. (2012) with permission

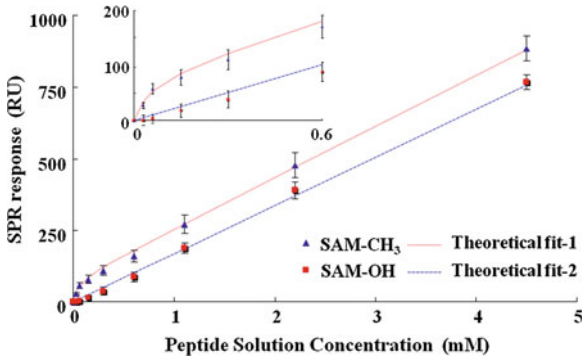

Fig. 3.2 Corresponding raw data adsorption isotherm for TGTG-V-GTGT on both of the SAM-CH_3 surfaces (*Triangle* experimental data fitted by Eq. (3.2): theoretical curve-1, *upper dotted line* $Q = 79$ (RU), $K = 19{,}300$ (unitless), and $m = 177{,}800$ (RU/M)) and SAM-OH [*white square* experimental data fitted by Eq. (3.2): theoretical curve-2, *lower dotted line* $Q = 0.24$ (RU), $K = 14$ (unitless), and $m = 168{,}000$ (RU/M)]. Note that the adsorption response plotted on the *y* axis includes bulk-shift effects, which are linearly related to solution concentration (*error bar* represents 95 % C.I., $N = 6$ in PBS.). Reprinted from Thyparambil et al. (2012) with permission

examples of sensorgrams from a set of SPR experiments for TGTG-V-GTGT peptides on a SAM surface, with the resulting adsorption isotherms from the raw sensorgram data presented in Fig. 3.2. ΔG^{o}_{ads} values for a set of peptides with 12 different X residues over a set of nine different functionalized SAM surfaces are presented in Table 3.3.

This SPR method could then be applied to investigate (i) the correlation between peptide adsorption affinity for SAM surfaces, as indicated by ΔG^{o}_{ads}, and the hydrophobicity characteristics of the SAM surfaces involved, and (ii) the influence of salt concentration on adsorption free energy. Figure 3.3 presents a plot of the of ΔG^{o}_{ads} values from Table 3.3 versus the respective cosine of the water

Table 3.3 Values of ΔG^{o}_{ads} (kcal/mol) for peptide-SAM combinations

-X-	–OH	–COOH	$–EC_3OH$	$–NH_2$	$–NHCOCH_3$	$–COOCH_3$	$–OC_6H_5$	$–OCH_2CF_3$	$–CH_3$
Nonpolar guest residues									
-L-	−0.003 (0.001)	−1.30 (0.43)	−0.40 (0.28)	−2.34 (0.80)	−1.04 (0.30)	−2.06 (0.31)	−2.68 (0.72)	−3.09 (0.31)	−3.87 (0.69)
-F-	*		−0.30 (0.13)	*	−2.44 (0.40)	*	*	−3.97 (0.24)	4.16 (0.16)
-V-	−0.002 (0.001)	−1.11 (0.31)	−0.26 (0.06)	−3.90 (0.12)	−0.16 (0.10)	*		−3.99 (0.22)	4.40 (0.31)
-A-	*		−0.97 (0.36)	*	*	*	*	*	*
-W-	−0.001 (0.001)	−1.14 (0.52)	−1.72 (0.33)	−2.71 (0.32)	−1.94 (0.45)	−0.92 (0.36)	−1.65 (0.60)	−3.42 (0.27)	−3.89 (0.34)
Polar guest residues									
-T-	−0.001(0.001)	−0.87 (0.46)	−0.28 (0.15)	−3.15 (0.50)	−0.16 (0.09)	−0.40 (0.14)	−2.89 (0.75)	−2.81 (0.40)	−2.76 (0.28)
-G-	−0.001 (0.001)	−0.68 (0.36)	−0.30 (0.20)	−2.56 (0.32)	−1.86 (0.20)	−1.18 (0.30)	−3.51 (0.22)	−3.30 (0.37)	−3.40 (0.39)
-S-.	002 (0.001)	−1.10 (0.10)	−0.34 (0.11)	−2.09 (0.98)	−1.49 (0.47)	−1.55 (0.26)	−3.20 (0.28)	−3.22 (0.24)	−2.75 (0.23)
-N-	−0.004 (0.003)	−0.86 (0.38)	−0.59 (0.11)	−3.22 (0.41)	−1.64 (0.23)	−1.37 (0.68)	−3.02 (0.16)	−3.41 (0.32)	4.33 (0.62)
Charged guest residues									
-R-	−0.002(0.001)	−1.53 (0.19)	−0 20 (0.10)	−3.03 (0.31)	−1.60 (0.80)	−1.17 (0.35)	−2.26 (0.82)	−3.45 (0.31)	4.15 (0.55)
-K-	−0.001 (0.001)	−1.71 (0.19)	−0.19 (0.07)	−3.14 (0.20)	−0.12 (0.07)	−1.77 (0.07)	−3.35 (0.25)	−3.54 (0.45)	−3.34 (0.39)
-D-	−0.003 (0.001)	−1.06 (0.09)	−0.44 (0.14)	−3.75 (0.20)	−1.93 (0.52)	−1.34 (0.50)	−3.89 (0.23)	−3.59 (0.37)	−3.54 (0.60)

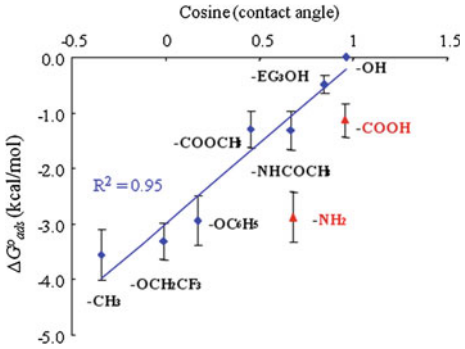

Fig. 3.3 ΔG^o_{ads} (kcal/mol) versus cosine (contact angle) for TGTG-X-GTGT on SAM surfaces with various functionalities in PBS. The ΔG^o_{ads} values represent the average value of all of the host–guest peptides that exhibited reversible adsorption behavior on each SAM surface (i.e., peptides with X = A, F, and V, which tended to adsorb effectively irreversibly, were excluded from these average values). The *blue line* shows the linear regression for the noncharged SAM surfaces with $R^2 = 0.95$ (the *error bar* represents 95 % C.I. with $N = 6$.) Reprinted from Wei and Latour (2009) with permission

contact angle values for each SAM surface (contact angle values are presented in Table 3.2). The ΔG^o_{ads} values shown in Fig. 3.3 represent the mean (±95 % C.I.) of the ΔG^o_{ads} values from all of the host–guest peptides that exhibited reversible adsorption behavior on each SAM surface (i.e., peptides with X = A, F, and V, which tended to adsorb effectively irreversibly, were excluded from these average values). The cosine of contact angle values here, which can be related to the free energy of displacement of water from the surface, provide an energetic scale for the peptide adsorption behavior on the different surfaces.

As clearly indicated in Fig. 3.3, the lowest mean ΔG^o_{ads} value (i.e., greatest adsorption affinity) was obtained on the SAM-CH_3 surface with the highest contact angle value and the highest mean ΔG^o_{ads} value (i.e., least adsorption affinity) was obtained on the SAM-OH surface with the lowest contact angle value (with greater cosine value). These results also clearly show that this general relationship holds for each of the neutrally charged SAM surfaces, with peptide adsorption affinity increasing (i.e., ΔG^o_{ads} gets more negative) in a manner that strongly correlates in a linear manner with the hydrophobicity of the SAM surfaces over the full range of contact angles. The physical meaning behind this linear relationship can then be understood as reflecting a thermodynamic benefit for the transition of interfacial water from the surface to the bulk water phase and a reduction in solvent accessible surface area of the system as the peptide adsorbs as the surface energy decreases (i.e., becomes more hydrophobic), resulting in a decrease in free energy (more negative ΔG^o_{ads}). However, in addition to this general linear trend shown in Fig. 3.3, the substantial amount of scatter around each data point from this trend line suggests that specific functional group interactions also substantially influence the adsorption behavior. This same general trend is apparent for the charged SAM

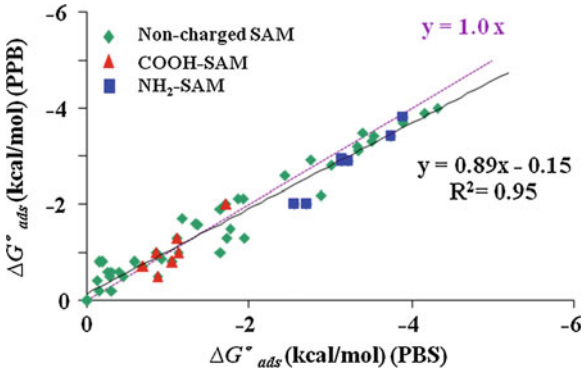

Fig. 3.4 Plot of ΔG^{o}_{ads} under PPB versus PBS solution conditions for 64 different peptide-SAM systems (peptides with X = V, G, F, W, K, D, T, and N, on eight different SAM surfaces [SAM-Y with Y = OH, CH_3, OC_6H_5, NH_2, COOH, $NHCOCH_3$, $COOCH_3$, and EG_3OH)]. The *solid line* represents a linear regression of the data points (regression equation in *black* text). The *dotted line* represents what the linear regression should be for perfect agreement between the two data sets (regression line in *purple* text with slope = 1.0 and *y*-intercept = 0.0). Reprinted from Wei et al. (2012) with permission

surfaces, but with an additional contribution of adsorption affinity due to the presence of relatively strong electrostatic interactions, which was expected based on the zwitterionic nature of each of the peptides.

To evaluate the influence of salt concentration on adsorption free energy, we then compared ΔG^{o}_{ads} values for peptide adsorption in PPB with our prior results obtained in PBS (Fig. 3.3). The resulting ΔG^{o}_{ads} comparisons between peptide adsorption in PPB versus PBS from SPR are presented in Fig. 3.4. As shown in Fig. 3.4, two lines are plotted in this figure: a solid line, which represents the linear regression of the experimental data points and a dotted line, which represents what the regression line would be if perfect agreement existed between the ΔG^{o}_{ads} values obtained in PPB compared with PBS, with a slope of 1.0 and y-intercept of zero. Statistical comparison between these two lines using a Student's t-test at the 95 % confidence level shows no significant difference in either the slope ($p = 0.12$) or the y-intercept ($p = 0.33$), thus indicating that the differences in salt composition and concentration between PPB and PBS do not substantially influence peptide adsorption behavior for this set of 64 different peptide–surface systems. Of particular interest, this finding holds for both the charged SAM surfaces (i.e., negatively charged COOH-SAM, red-triangle data points; and the positively charged NH_2-SAM, blue-square data points) as well as for the noncharged SAM surfaces (green diamond data points). This observation primarily indicates that the presence of monovalent Na^+ and Cl^- salt ions in solution from 0 to 140 mM concentration in the presence of 10 mM phosphate buffer has negligible influence on peptide adsorption behavior.

These results provide a quantitative measure of peptide adsorption behavior at a liquid–solid interface as a function of amino acid type and surface functionality,

thus providing fundamental insights for understanding peptide and protein adsorption behavior for applications in bionanotechnology and biomedical engineering.

3.4.5 Determination of Effective ΔG^o ads Using a Standardized AFM Method

As noted above, the use of experimental techniques such as SPR for the determination of ΔG^o_{ads}, is limited to use for materials that can readily form nanoscale-thick layers over sensor surfaces, thus limiting these techniques to a relatively small set of materials. In order to provide a means of obtaining values of ΔG^o_{ads} for a much broader set of materials (i.e., surfaces that are not conducive for use with techniques such as SPR), we have developed a standardized AFM method that can be applied to any macroscopically smooth surface for the determination of effective ΔG^o_{ads} values by correlating the force of desorption measured by AFM with ΔG^o_{ads} values measured by SPR.

The desorption force for peptide–surface interactions (F_{des}) is measured from force curves using an AFM instrument (MFP-3D instrument, Asylum Research, Santa Barbara, CA) with DNP-10 silicon nitride cantilevers (Veeco Nanofabrication Center, Camarillo, CA) at room temperature in a fluid cell filled with droplets of either PPB or PBS, pH 7.4. For this technique, our TGTG-X-GTGT host–guest peptides are modified to TGTG-X-GTCT to provide a cysteine amino acid that is used to link the peptides to the AFM tips. The modified host–guest peptide sequences are tethered to AFM tips via a heterobifunctional PEG tether (3.4-kDA pyridyl dithio propionate-poly(ethylene glycol)-*N*-Hydroxyl succinimidyl ester (PDP-PEG-NHS), Creative PEGWorks, Winston Salem, NC), the specific details of which have been published (Wei and Latour 2010). Tips with PEG–OH (i.e., without the peptide) are then also used as controls. Although there is uncertainty in the areal density of tethered peptides on the probe tip, as long as the AFM force measurements for peptide–surface interactions are obtained using a standardized methodology, similar probe tip densities (although unknown) can be expected (Thyparambil et al. 2012). The functionalized tip with the peptide is then brought in contact with a selected substrate surface for one second of surface delay and then retracted at a constant vertical scanning speed of 0.1 μm/s. The peptide–surface interaction force is then recorded as a function of the tip-to-sample separation distance on approach and retraction. From this data for each peptide–surface combination, the unbinding force that is measured during the plateau region ending right at the separation distance (max sep), which corresponds to the contour length of the PEG spacer and the peptide sequence, is taken as the F_{des}, as illustrated in Fig. 3.5 (Horinek et al. 2008; Pirzer et al. 2009).

In order to apply this method for the determination of effective values of ΔG^o_{ads}, AFM studies were first conducted to measure F_{des} for a set of eight different types

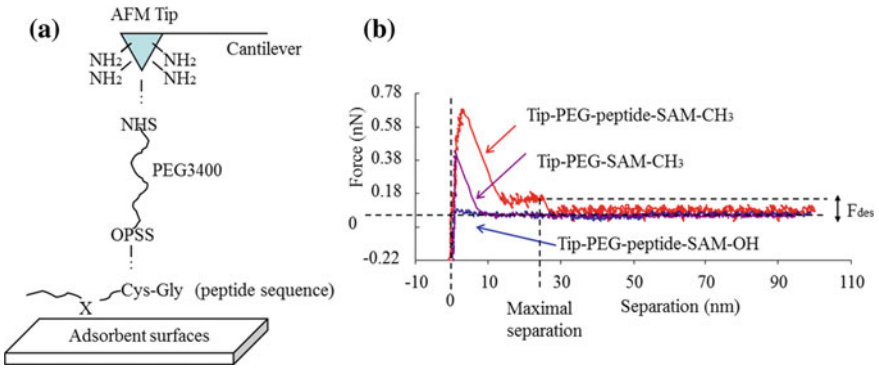

Fig. 3.5 **a** AFM tip linkage. Peptide sequences are coupled to AFM tips via a 3.4 kDa polyethylene glycol (PEG) crosslinker. **b** AFM force–separation curves recorded during adsorption–desorption of TGTG-V-GTCT peptide on a SAM-CH_3 (*upper red curve*) and an SAM-OH (*bottom blue curve*). The *middle* (*purple*) curve represents a control group with the AFM tip without the peptide (only covered with PEG) on a SAM-CH_3 surface. Reprinted from Wei and Latour (2010) with permission

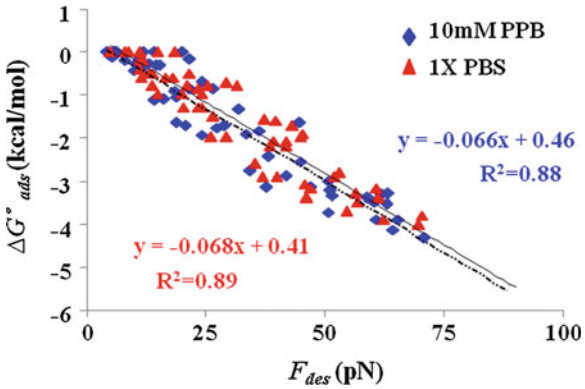

Fig. 3.6 Correlation between $\Delta G^{o}_{\text{ads}}$ by SPR and F_{des} by AFM for an equivalent set of 64 peptide-SAM systems in PBS (*lower dashed* trend line with $R^2 = 0.89$; *red triangle* data points and *red* regression equation) and 10 mM PPB (*upper solid* trend line with $R^2 = 0.88$; *blue diamond* data points and *blue* regression equation); pH = 7.4, 25 °C. Reprinted from Wei et al. (2012) with permission

of peptides on a set of eight different types of SAM surfaces in PBS and 10 mM PPB that were also evaluated by SPR (Fig. 3.4).

As shown in Fig. 3.6, a strong linear correlation (dashed trend line with $R^2 = 0.88$; blue-diamond data points) is observed for the 64 peptides-SAM systems in PPB in a manner that is essentially indistinguishable with the linear relationship found with the dataset in PBS (solid trend line with $R^2 = 0.89$; red-triangle data points). Comparison between regression lines for the datasets in PBS and PPB

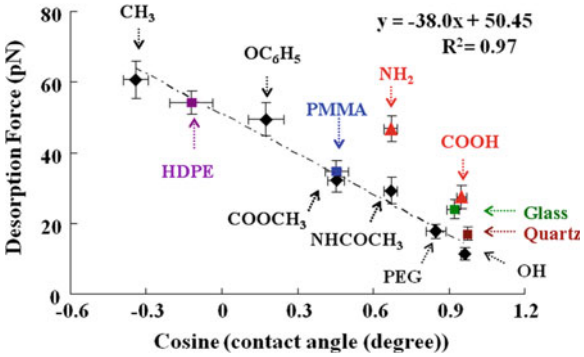

Fig. 3.7 F_{des} versus cosine (static water contact angle) for SAMs with specific functionalities and the selected material (Snyder et al. 2012; Thyparambil et al. 2012; Wei et al. 2012). The trend *line* shows the linear regression for the noncharged surfaces (i.e., excluding the charged SAM and material surfaces at pH 7.4: SAM-NH_2 (pK ~ 6.5) (Fears et al. 2008) and -COOH (pK ~ 5.5) (Jiang et al. 2002) and the glass and quartz surfaces which were expected to be negatively charged (Sabia and Ukrainczyk 2000). The *error bars* represent the 95 % C.I. with $N = 48$ for F_{des} and $N = 3$ for contact angle measurements

again shows no significant difference in either the slopes ($p = 0.68$) or intercepts ($p = 0.19$) at the 95 % confidence level ($\alpha = 0.05$), thus indicating negligible influence of the differences in the salt compositions and concentrations between these two solution environments along with consistency in the correlation between F_{des} measured by AFM and $\Delta G^{o}_{\text{ads}}$ determined by SPR using the applied experimental methods. A combination of these two datasets provides an overall correlation equation (Eq. (3.4)) with $R^2 = 0.89$.

$$\Delta G^{o}_{\text{ads}} = -0.067\, F_{\text{des}} + 0.44 \tag{3.4}$$

Equation (3.4) thus provides the means to determine effective values of $\Delta G^{o}_{\text{ads}}$ for material surfaces that are not readily amenable for use with SPR by conducting measurements using our standardized AFM method to measure F_{des} and then applying this correlation equation to estimate $\Delta G^{o}_{\text{ads}}$ for these systems in either PPB or PBS solution. This capability is of interest to provide a common basis for comparing peptide interactions for a broad range of material surfaces that can be tested by either SPR (e.g., SAMs, some thin polymer films) or AFM (e.g., glass, quartz (100), HDPE, and PMMA).

The reasonableness of applying this newly developed $F_{\text{des}} : \Delta G^{o}_{\text{ads}}$ correlation to estimate the $\Delta G^{o}_{\text{ads}}$ for peptide–surface systems can be generally assessed by plotting the measured F_{des} values to the cosine of the static water contact angle of these surfaces along with the SAM surfaces as an additional check on the validity of these results (Fig. 3.7) (Thyparambil et al. 2012). As shown, the relationship between the cosine of the static water contact angle and F_{des} for this set of additional material surfaces (HDPE and PMMA) agrees extremely well with the

data for the noncharged SAM surfaces. A strong correlation exists between F_{des} and the water contact angle for each of the neutrally charged SAM surfaces, with peptide adsorption affinity increasing in a linear manner with the hydrophobicity of the SAM surfaces over the full range of contact angles. For the charged SAM surfaces (e.g., SAM-NH_2 and –COOH) and the silica glass and quartz samples, the strength of adsorption is substantially higher than the correlation line for the noncharged surfaces, reflecting the additional attraction considered to be provided by electrostatic interactions between the peptides and the surfaces, similar to what we have observed from our previous SPR data set shown in Fig. 3.3. The correlation between the peptide desorption force and the cosine of the static water contact angle thus provides an additional means of qualitatively assessing the reasonableness of the AFM desorption force results prior to using the data to estimate $\Delta G^{o}_{\text{ads}}$ for a given peptide–surface system.

These synergistically combined methods thus provide the ability to make quantitative measurements of peptide–surface interactions for any macroscopically flat surface, including surfaces that are not amenable for use with SPR. Importantly for our specific interests in the development of methods to accurately predict peptide and protein adsorption behavior, these methods also provide a means to obtain experimental data that are useful for the evaluation, modification, and validation of interfacial force field parameters that are required to enable peptide and protein adsorption behavior to be accurately represented by molecular simulation (Latour 2008; Vellore et al. 2010; Snyder et al. 2012).

3.4.6 Concluding Remarks for SPR and AFM Methods

The above-described combined SPR and AFM methods provide experimental approaches to obtain thermodynamic properties for the characterization of peptide–surface interactions that can be used with any macroscopically flat material surface. If appropriately applied, these methods are able to generate very accurate and reproducible determinations of adsorption free energy. While these techniques have utility for a broad range of applications, they are limited in terms of not being applicable for the characterization of peptide interactions with nano- and microsized particles, which are of particular interest in the general area of nanobiotechnology and for drug delivery systems in biomedical engineering. Fortunately, alternative methods are available for the determination of thermodynamic parameters for these types of systems. One of the most powerful methods for this type of application is ITC. Using ITC, the change in energy due to peptide–surface interactions can be directly measured over a range of temperatures, from which adsorption-induced changes in enthalpy, entropy, and free energy can be readily determined. The fundamentals of ITC and its application for a range of molecular systems are addressed in the following section of this chapter.

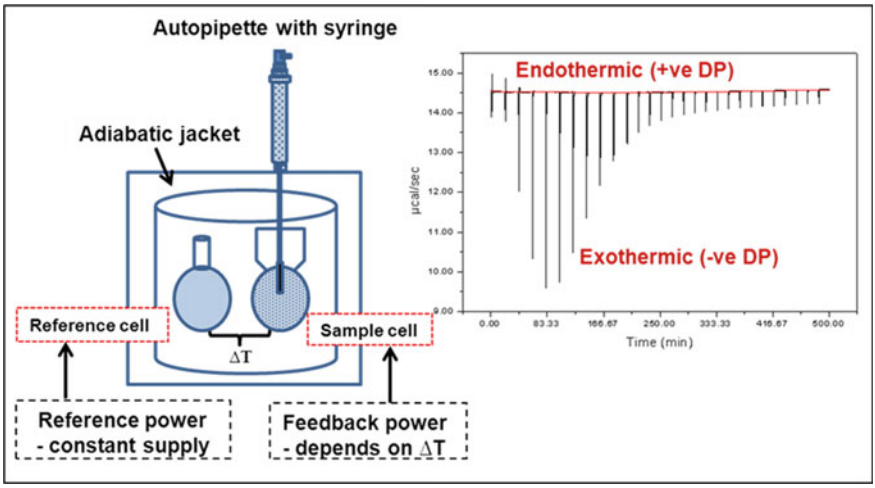

Fig. 3.8 A simplified diagram of an ITC instrument showing its components and a representation of raw data

3.5 Isothermal Titration Calorimetry

The chemical or physical interaction of any two components forming a complex is accompanied by an exchange of heat with the environment, with heat either being absorbed (endothermic) or released (exothermic). The complex may also further undergo a physical change forming a product in a process which also produces a heat change. Modern ITC instruments are powerful precision devices designed to use power compensation to monitor heat changes that occur when two components interact. An ITC consists of a reference cell and a sample cell which are enclosed in an adiabatic outer shield jacket (Fig. 3.8). The cells are made using chemically inert and thermal conducting material such as Hastelloy alloy used in VP–ITC MicroCal instruments (MicroCal 2003). The reference cell should contain the solvent in which the component in the sample cell (i.e., macromolecule) is dissolved or suspended in. An important component of the instrument is its automated pipette containing a syringe which is filled with a second component (i.e., ligand) dissolved in the same solvent used to fill the reference cell and containing the component in the sample cell.

At the start of a measurement, the temperature of the reference cell and the sample cell is at equilibrium. A reference power which is defined by the user is constantly supplied to the reference cell offset heater to maintain a positive differential power (DP) feedback system also acknowledged as the baseline setting (thermal equilibrium). The positive DP can be used to supply compensating power to the sample cell whose temperature changes when a component from the syringe is titrated into the sample cell containing another component with which it is expected to interact. Differences in temperature between the sample cell and the

reference cell are monitored using a sensitive thermocouple circuit throughout the experiment. The extent of heat change depends on whether an interaction occurs or not. If no interaction takes place, only heat change as a result of titrating the syringe component into the sample cell component is measured which may be similar to the dilution heat change of titrating the syringe component into the sample cell containing only the solvent. However, if an interaction occurs forming a complex, a greater heat change than dilution heat change occurs causing the sample cell to be either hotter or cooler than the reference cell. If the sample cell is hotter than the reference cell (exothermic reaction) less power will be required to maintain thermal equilibrium between the two cells thus a negative DP (μcal/s) will be registered. The opposite happens if the sample cell is cooler than the reference cell (endothermic reaction), more power will be required to maintain thermal equilibrium hence a positive DP will be recorded. The heat signal/power required to return to thermal equilibrium is integrated with respect to time and is directly proportional to the amount of interaction that occurs (Cliff et al. 2004).

The total volume of the component in the syringe can all be injected slowly and continuously into the sample cell component in what is known as the single injection method (SIM). However, the conventional ITC method involves the injection of the total syringe volume in several small aliquots of known volume. With continuous addition of the syringe component into the sample cell component, the cell component eventually becomes saturated at which point the heat signal decreases until only dilution heats are observed (Liang 2008; Thomson and Ladbury 2004). The extent of the reaction can, therefore, be probed per injected aliquot and this heat signal can be described as apparent ΔH (ΔH_{app}) or observed ΔH (ΔH_{obs}) heat change which is a global response as it includes the sum total of all heat changes. Total heat change is attributed to (i) noncovalent (hydrogen bonding, electrostatic interactions, hydrophobic interactions and van der Waals forces) binding/interaction (ΔH_{bind}) which principally reflects the strength of the interaction (ii) other contributions to heat change such as protonation/deprotonation events (ΔH_{ion}), and (iii) conformational changes as well as the incorporation or displacement of solvent both of which are reflected in the ΔS of the interaction (Ababou and Ladbury 2006; Cliff et al. 2004; Leavitt and Freire 2001).

Data analysis can be carried out with the help of software such as Origin to plot and fit data using suitable binding models made available by MicroCal that use a nonlinear least-squares algorithm. After subtracting the baseline experiment (dilution heat change) from the ligand binding experiment, data is plotted as normalized integrated heat change in kcal/mole of injectant against the molar ratio of ligand to macromolecule to obtain the binding isotherm. The equilibrium binding constant (K_B) can then be determined from precise knowledge of the concentration of free and bound ligand. The accuracy of K_B can be evaluated based on a measurement known as the critical parameter (C) which determines the shape of the isotherm and is a product of the total concentration of the cell component, K_B and the stoichiometry (n) and should ideally lie between 10 and 100 (Cliff et al. 2004). The stoichiometry value (n) represents the number of binding sites per particle or macromolecule for a specific ligand. Figure 3.9 shows the effect of

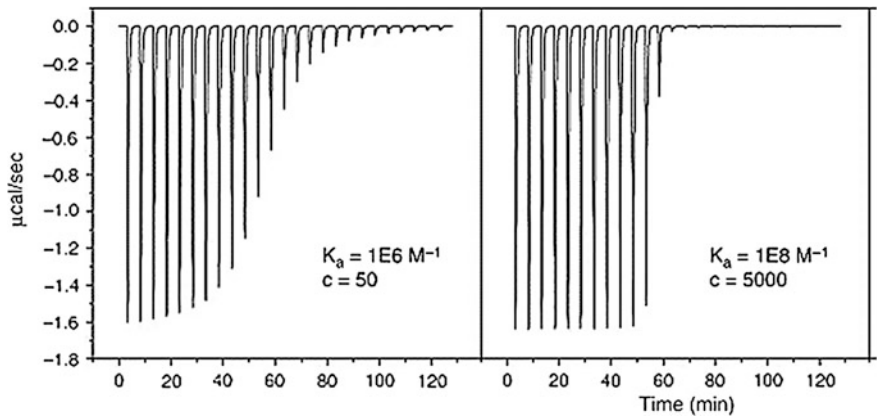

Fig. 3.9 Illustration of the interaction between a protein and a ligand showing the effect of increasing the binding affinity measured in ITC experiments. Critical parameter (C) = K_B × protein concentration × n. Experiment parameters used were: cell volume of 1.4 ml, 10 µl injection aliquots, protein concentration of 0.05 mM, ligand concentration of 0.6 mM, ΔH_{bind} = −10 kcal/mol, and n = 1. Where C = 50 in the first panel, K_B and ΔH can be determined accurately but in the second panel where C = 5,000 only ΔH can be determined accurately. Reprinted with permission from Leavitt and Freire (2001) Elservier

increasing the binding affinity hence the C value on the shape of isothermal profiles obtained using an ITC (Leavitt and Freire 2001). C values lower than 10 have featureless curves to almost straight lines which imply that there is very little change in enthalpy from one injection to the next hence determining the concentration of bound and free ligand becomes erroneous. On the other extreme scenario where C values are higher than 100, the shape of the isotherm tends toward an angular form as saturation occurs too fast in the first few injections equally precluding accurate determination of K_B (Cliff et al. 2004; Leavitt and Freire 2001; Thomson and Ladbury 2004; Wiseman et al. 1989).

From ΔH and K_B, other thermodynamic parameters of interaction; entropy (ΔS) and Gibbs free energy (ΔG) can then be determined using Eq. (3.5) below where T is the experimental temperature and R is the gas constant (Cliff et al. 2004; Karlsen et al. 2010; Thomson and Ladbury 2004).

$$\Delta G = \Delta H - T\Delta S = -RT\ln K_B \tag{3.5}$$

ITC is, therefore, a powerful technique able to determine all thermodynamic parameters of interaction from one experiment and is the only direct measure of molar enthalpy (Cliff et al. 2004). It is a highly sensitive tool that can measure as little as 0.1 µcal heat change and can determine binding constants in the millimolar to picomolar range (10^2–10^9 M^{-1}). Additional advantages are that ITC does not require labeling or immobilization of the interacting components. These features make it superior to other conventional techniques used to measure binding constants of interaction such as SPR, quartz crystal microbalance with dissipation

monitoring (QCM-D), nuclear magnetic resonance (NMR), spectroscopy, analytical ultracentrifugation (AUC), stopped-flow, and radioligand binding assays; many of which would require a series of experiments at different concentrations and temperatures before thermodynamic parameters can be determined using Van't Hoffs equation (Ababou and Ladbury 2006; Chaid et al. 2009). All the above techniques have advantages and disadvantages outlined elsewhere in the literature but a combination of complementary techniques is highly beneficial (Chaid et al. 2009; Mahmoudi et al. 2011).

3.5.1 ITC and Peptide–Surface Interactions

ITC was initially developed for the study of biological binding interactions mainly biopolymer interactions such as protein–enzyme interactions and DNA (deoxyribonucleic acid)-protein interactions (Ababou and Ladbury 2006; Biltonen and Langerman 1979; Wiseman et al. 1989). Over the years, commercial instruments have been designed with improvements in sensitivity, controlled and accurate automation of experiment, faster response, and advanced data analysis software (Freyer and Lewis 2008; Perozzo et al. 2004). Its applications are continuously being expanded and it is now being used in other fields such as in materials science to study thermodynamics of interfacial interactions between various inorganic and organic components (Ababou and Ladbury 2006; Chiad et al. 2009; Joshi et al. 2004).

Biomolecules such as carbohydrates, proteins, and lipids are known to play significant roles in biomineralization processes (Dujardin and Mann 2002; Kroger et al. 1999). Proteins in particular have sparked great interest due to their exceptional properties of specificity, biofabrication, self-assembly, recognition, and their ability to control the biosynthesis of soft through to hard biomaterials having detailed structural motifs at the nanoscale (Davis et al. 2003; Perry et al. 2009; Sanford and Kumar 2005). Peptide sequences which can interact specifically with any target surfaces, not just biomaterials have been identified using combinatorial methods such as the phage display technique and more recently, computational tools are also being employed (Dickerson et al. 2008; Naik et al. 2002; Oren et al. 2005; Sarikaya et al. 2003). In some cases, these peptide sequences not only interact with the target surface but have also been seen to modify the structure of the material which is believed to occur through modification of energy barriers at the peptide–surface interface (Cedervall et al. 2007; Dickerson et al. 2008; Naik et al. 2002; Perry et al. 2009; Whyburn et al. 2008). The exact nature of the interactions between inorganic materials and peptides remains largely elusive. Understanding the changes that occur at the interface during peptide–inorganic interactions and correlating these to structural modifications of the inorganic materials could be the key to advancing material synthesis and design.

In general, peptide adsorption on inorganic surfaces may be influenced by three overriding factors: (i) the intrinsic properties of the peptide (ii) the physicochemical properties of the inorganic surface, and (iii) the media/environment

where the interaction takes place. Interaction may occur through specific counterparts (reactive groups) that allow only certain peptide sequences to interact specifically with certain inorganic surfaces and not others as demonstrated using the phage display technique. The inherent characteristics of the peptide sequence that may play a role in determining whether an interaction takes place with a substrate are mainly its charge, hydropathy, and conformation. The overall net charge of the peptide mainly influences the occurrence of electrostatic interactions or repulsion with a surface that may also be charged. Many studies have attributed electrostatic interactions as the principle driving force behind peptide–inorganic interactions (Lynch and Dawson 2008; Chen et al. 2011). However, other non-covalent interactions such as hydrophilic or hydrophobic interactions, van der Waals forces, and hydrogen bonding between peptides and a surface are equally significant and may singlehandedly drive interactions in conditions where peptides have no net charge or even under repulsive charge conditions (Lynch and Dawson 2008; Rezwan et al. 2005). The media in which the interaction is taking place influences the conformation and stability of the peptide which may structure itself depending on its properties, mainly the hydropathy of individual amino acids and/or the specific alignment of amino acids in the sequence relative to the polarity of the media. The overall binding activity of the peptide against the surface may depend on a contribution from various chemical and physical parameters. Ultimately, the interaction may be reversible or irreversible attained through a contribution from many weak interactions. Hence, some questions that need to be explored in the study of peptide–inorganic interactions include:

- What are the intrinsic properties of the peptide sequence and what are the differences between the free and bound states of the peptide?
- What are the surface properties of the inorganic material in solution (media) and what changes take place on the surface before a peptide molecule adsorbs onto it?
- What forces drive the interaction between a specific peptide and an inorganic material? What is the strength and reversibility of the interaction, how do these interactions modify the energy barriers at the peptide–inorganic interface and eventually lead to morphology modification of inorganic materials?

ITC is potentially the most ideal technique to study peptide–surface interactions as it can be used to directly determine all thermodynamic parameters of interaction. However, its application to study peptide–surface interactions is at its infancy with few documented studies in literature to date. This approach has its challenges which cannot go unmentioned.

In a typical ITC experiment to characterize the interaction of a ligand with a receptor, an interaction occurs forming a ligand–receptor complex described by E. Fisher as a lock and key mechanism. The formation of the complex is accompanied by a heat change as a result of binding but may also include a contribution from solvation entropy and structural changes (i.e., conformational change of the ligand in solution before it interacts with the receptor, structural changes of the

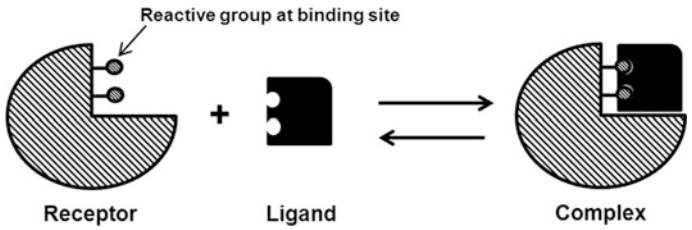

Fig. 3.10 A simplified model of a specific interaction between a ligand and a receptor forming a complex

receptor to accept the ligand and the final ligand-receptor complex may also undergo conformational changes). The receptor-binding site is specific as it is defined by a precise geometry/recognition motif and the interaction is achieved through chemical functions at the binding site through which it can complex to the ligand (Ball and Maechline 2009). This interaction is at a reversible equilibrium hence the free energy change can be measured experimentally through determination of the K_B (Fig. 3.10).

ITC studies of peptide–inorganic interactions differ from typical ITC experiments. For example, here the inorganic material is a solid entity, therefore, any conformational entropy that may contribute to the measured heat change can only result from differences between the free and bound peptide. Also determination of K_B requires that precise concentrations of the initial free peptide and binding site on the inorganic surface to be known. The peptide concentration can be determined accurately if all quantified peptide is pure and active; however, clearly defining and quantifying the binding site on the inorganic surface is more challenging. For instance, synthesis studies of inorganic materials in the presence of peptides showing morphology modification via the adsorption growth inhibition mechanism have demonstrated that in some cases, peptides adsorb preferentially or solely to specific crystal planes (Chiu et al. 2011; Liang et al. 2011; Togashi et al. 2011). Adsorption of proteins on a surface of an inorganic material is described by some as nonspecific as there may be no clearly defined recognition pattern on the surface of the inorganic material similar to the lock and key mechanism (Ball and Maechline 2009). However, few studies have defined recognition Patterns in peptide–inorganic surface interactions such as in studies of interaction between platinum (Pt) binding peptides with Pt crystallographic surfaces (Oren et al. 2005; Ruan et al. 2013). Computational analysis suggested the occurrence of physical recognition when platinum metal-binding peptides came into contact with the crystallographic metal surfaces (Oren et al. 2005; Ruan et al. 2013). The binding site can, therefore, be defined as the physicochemical characteristics of the inorganic material surface that can be recognized by the reactive groups present on the peptide sequence that form the “hot spot” regions through

which the interaction can take place. The importance of thorough characterization of peptides and inorganic materials used in such studies, therefore, becomes paramount and will be discussed hereafter.

3.5.2 Characterization of Peptides and Inorganic Particles for ITC Experiments

Peptide sequences identified from combinatorial methods or computational tools can be synthesized using microwave-assisted solid phase peptide synthesis protocol and their concentration, purity, and molecular weight can be ascertained using High performance liquid chromatography (HPLC), UV spectrophotometry, and Mass spectrometry. Circular dichroism (CD) and computational tools such as GROMACS, NAMD, Tripos SYBYL, and Accelyrys Materials studio can be used to study the conformation and stability of peptide sequences. Dynamic light scattering (DLS) and zeta potential measurements can be used to study the size, dispersity, and net charge of peptides in solution. The net charge and isoelectric point of the peptides can also be calculated using the Henderson–Hasselbalch equation.

Inorganic particles can be synthesized using various techniques including: hydrothermal synthesis, template-directed approach, sol–gel process, electrospinning, electrodeposition, chemical vapor deposition, vapor phase transport process, and pyrolysis. Hydrothermal synthesis is carried out under ambient reaction conditions and is therefore commonly used in biomimetic studies. Physicochemical properties of inorganic surfaces that need to be determined include the surface charge, hydrophilicity/hydrophobicity, nanotopography, surface chirality, surface curvature, reactive sites, and stability of the surface/dissolution. These aspects have been covered in detail in a recent review (Fenoglio et al. 2011). Inorganic particles can be functionalized using different ligands and various organic capping agents including peptides are used to control the growth and morphology or inorganic particles. In circumstances where the interest is to study interactions of molecules with functionalized nanoparticles, the characteristics of the nanoparticles imparted by the ligand used to modify them should be known (Huang et al. 2013; You et al. 2008). Where the interest is to thermodynamically characterize interactions of molecules with bare nanoparticles, ideal particles should be pure, monodisperse, and homogeneous, having identical morphology of controlled shape and size. Attaining such particles is challenging and continues to be pursued by many researchers including ourselves. In this case, if capping agents were used during synthesis they have to be removed.

In our studies, we applied ITC to study the interaction of metal oxide and metal surfaces with peptides that had been shown to modify the morphology of the inorganic materials during synthesis studies (Chiu et al. 2011; Liang et al. 2011; Tomczak et al. 2009). As an example, we have monitored interactions between

ZnO crystals and ZnO-binding peptides using ITC. ZnO crystals used in ITC experiments were synthesized in the presence of organic matter either as precursors, solutes such as bases or growth modifying additives like peptides which can tightly adsorb to ZnO crystal planes. It was, therefore, crucial to characterize the organic content of the material before use in interaction studies with peptides. ZnO is known to decompose at a temperature of about 1,975 °C (Oka et al. 2002). ZnO-based materials can therefore be safely calcined to 900 °C to remove all organic materials. At 900 °C, there was also little risk of phase transformation of the ZnO crystals as this is known to require temperatures above 1,300 °C (Mazaheri et al. 2008). Synthesized particles were calcined up to 900 °C and weight loss was monitored by thermogravimetric analysis (TGA). Even though the crystals had been washed after synthesis, TGA analysis showed that ZnO crystals, even those formed without additives still contained a small amount of surface adsorbed organic matter (1.64 % ± 0.21). In our syntheses, the organic matter was identified to be an intermediate compound, layered basic zinc salt formed during the synthesis process. Calcined ZnO precipitates were again characterized using scanning electron microscopy (SEM) and appeared to have maintained their structure. X-ray diffraction (XRD) analysis confirmed that no phase transformation had taken place.

In another study within our group of the interaction of platinum-binding peptides and platinum nanoparticles, monodisperse cubic Pt nanoparticles with the {100} phase crystal structure were needed. Pt nanoparticles were prepared from a precursor using a growth modifying capping agent poly(vinylpyrrolidone) (PVP) along with trace levels of silver ions to enhance the rate of crystal growth along the desired plane (Song et al. 2005). The synthesized Pt nanoparticles cleaned according to the protocol described by Song et al. (2005) showed a significant amount of organic matter greater than 10 % weight content which was not desired for interaction experiments of Pt with Pt-binding peptides. As it is known that strongly bound PVP or any other capping agent can be challenging to remove (Rioux et al. 2006) an alternate approach to nanoparticle cleaning including calcination (not ideal for unencapsulated Pt nanoparticles as it leads to aggregation), plasma, or UV–ozone cleaning and the use of chemical cleaning methods for nanoparticles was required (Crespo-Quesada et al. 2011; Monzó et al. 2012). Most chemical cleaning methods are specific for a particular capping agent. For the removal of PVP from Pt nanoparticles, a method using a mixture of H_2O_2 and H_2SO_4 described by Monzó et al. (2012) was similarly used in our studies. TGA analysis was then used to confirm removal of the unwanted organic matter and the free-flowing state of the nanoparticulate (required for ITC analysis) confirmed using transmission electron microscopy (TEM). Any effects of contamination from Ag species was assessed by a combination of energy-dispersive X-ray spectroscopy (EDX), inductively coupled optical emission spectroscopy (ICP-OES), and XRD analysis of the treated platinum nanoparticles.

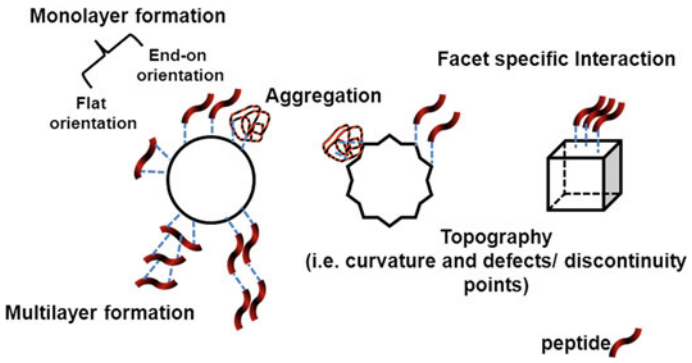

Fig. 3.11 Illustration of some possible peptide–surface and peptide–peptide modes of interaction. Peptides may interact with the inorganic materials using specific functional groups of the amino acids in the sequence which may recognize chemical/physical surface features of the inorganic material. Image is not drawn to scale

In brief, some techniques that can be used to characterize the nanoparticulates include the use of imaging tools such TEM and SEM to characterize the morphology (shape, size, and aggregation) of the inorganic material. X-ray photoelectron spectroscopy (XPS) and EDX can be used to determine the samples' elemental composition. X-ray diffraction can be used to structurally characterize samples distinguishing between amorphous and crystalline samples. DLS and zeta potential measurements can be used to determine the hydrodynamic radius and surface charge of nanoparticles. The surface area of inorganic materials can be determined using nitrogen gas adsorption with analysis of the data using the Brunauer–Emmett–Teller (BET) method or calculated from dimensions obtained from image analysis such as SEM and TEM.

Quantifying the binding sites on the inorganic particles is complicated by the possible different adsorption orientations of peptide molecules (i.e., end-on surface adsorption, flat-on surface adsorption, adsorption as a monolayer, or multilayers and aggregates formed through possible peptide–peptide interactions) and possible surface specific adsorption whereby peptides adsorb to specific sites and not the total surface area (Fig. 3.11). These parameters are challenging to determine and require a combination of several complementary techniques and methodologies to ascertain. Once more, questions arise about the stability of the peptide–inorganic particle adduct; How dynamic or static is the adsorbed layer, whether a soft (weak and reversible interaction) or a hard (strong and irreversible) peptide layer adsorbs? The binding process is driven by kinetic and thermodynamic factors and may also vary depending on the properties of the peptide, the inorganic surface, the concentrations used, and temperature of the interaction environment as well as the influence of other molecules, including other ions and buffers present in the media.

3.5.3 Basic Steps to Planning and Conducting an ITC Experiment

This section has been written as a practical guide for ITC users. Herein, the instrument referred to is a MicroCal VP–ITC developed by GE Healthcare but the principles can be transferred for use with other similar ITC instruments. Before setting up an ITC experiment, the conditions under which the experiment should be conducted should be considered. VP–ITC has been set up to allow the user to alter a number of experimental parameters to optimize an experiment. These are the total number of injections, cell temperature (°C), reference power (μcal/s), initial delay (s), syringe concentration (mM), cell concentration (mM), and stirring speed (rpm). Optimization is conducted to (i) attain saturation (which indicates the endpoint of the reaction), (ii) to minimize dilution heats in order to avoid interference in heats measured, and (iii) to attain sufficient measurements between baseline and saturation for prediction of curve shape. The importance of curve shape will be highlighted shortly.

3.5.3.1 Experimental Parameters

For the study of peptide–inorganic particle interactions using ITC, when working with a suspension of particles, it is best to have the nanoparticles in the sample cell as opposed to the syringe to avoid obstructing the flow and dispelling incorrect volumes into the sample cell during the experiment or completely blocking and damaging the syringe. Additionally, it is beneficial to have the particle suspension in the sample cell as the entire assembly of the syringe can be rotated continuously throughout the experiment maintaining the particles in suspension, availing all possible binding sites for the ligand. A stirring speed of 270–310 rpm (revolutions per minute) is usually optimal. However, when working with particles or if the solutions being mixed are viscous, it is recommended by MicroCal that the stirring speed should be fast enough to reduce error that can be encountered at the equivalence point of extremely tight interactions if the injected ligand is not evenly mixed throughout the cell component but should not be too fast to the point where the baseline becomes too noisy.

For a VP–ITC instrument, the user can chose to maintain the cell temperature between 2 and 80 °C. The temperature of the reaction affects the heat of binding and the binding constant. The instrument should be in a temperature controlled environment as fluctuation in room temperature may influence its performance and maintenance of cell temperature. At the start of the experiment, a thermal equilibrium is established which is the baseline of the experiment and falls around the value of the chosen reference power. MicroCal recommends a reference power of about 15–20 μcal/s for systems where there is no prior knowledge of the expected heat change. For large endothermic heat changes, a low reference power ($\sim$2 μcal/s) is sufficient whereas for large exothermic heat changes, a large

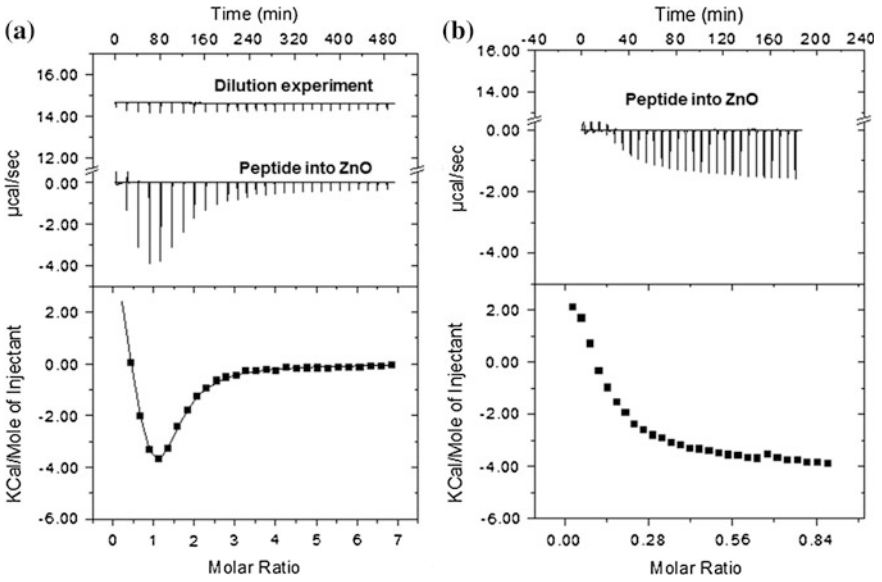

Fig. 3.12 ITC isotherms representing heat changes that occur as a result of peptide GT-16 (GLHVMHKVAPPR-GGGC) interacting with ZnO hexagonal rods of wurtzite crystal structure, L/DAvg 8.92 ± 3.26. **a** *Above*, raw data profile of titrating 280 µl of 3.125 mM GT-16 peptide in 10 µl aliquots into a cell containing 1.4 ml of ddH_2O producing heats of dilution. *Below*, raw data profile of titrating the peptide into a cell containing a suspension of 0.1 mM ZnO rods (0.1 mM Zn^{2+} determined using ICP-OES). Saturation is reached and both endothermic and exothermic heat change is measured. Dilution heat change has been subtracted. **b** GT-16 (1.25 mM) into an ITC cell containing a suspension of 0.3 mM ZnO rods. Saturation is not attained and heat measured is predominantly endothermic. A constant cell temperature of 298 K was maintained in all experiments. (Unpublished data)

reference power (~30 µcal/s) may be required. An Initial delay (s) is required before the first injection to collect the baseline data.

The shape of the titration curve is important for determining K_B and is controlled by the concentration of the interacting components in the cell (molar ratio of ligand and macromolecules). Figure 3.12 illustrates how the molar ratio of the syringe and sample cell component determines the observed heat change and curve shape in an interaction where there are two thermodynamic events, an endothermic and an exothermic interaction.

The autopipette functions allow the user to control injection parameters such as the volume (µl) dispensed from the syringe into the cell per injection, the duration (s) it takes for each injection to be made, the spacing (s) in between two subsequent injections which should be sufficient to allow thermal equilibrium to be re-established after each injection and the filter period (s), which is the period in which data collected is averaged and a single data point produced and plotted.

3.5.3.2 Sample Preparation and Running an ITC Experiment

The desired peptide concentration and nanoparticles required for each experiment are prepared in the chosen media. When choosing the media, the operator should be aware of the material used to make the ITC cell. For a MicroCal VP–ITC instrument, the cell is made using Hastelloy® C-276 alloy which is a robust material capable of withstanding corrosion by strong bases. However, strong acids can destroy the material and should therefore not be used. Hence any nonacidic solvent can be used in ITC experiments. The user should choose the most suitable solvent (it can be a mixture of solvents) that best dissolve the ligand/macromolecule and/or best disperse the inorganic particles (Chiad et al. 2009).

Generally, ITC experiments are conducted in aqueous media i.e., water and buffer (Bouchemal and Mazzaferro 2012). However, if nonaqueous or organic solvents is required, one has to ensure that the heat of dilution is minimal not to interfere with the accuracy of the binding experiment especially where the heat change of binding is comparatively minute (Thomson and Ladbury 2004). When buffers are used, buffer related contributions to the observed heat change should be considered (Leavitt and Freire 2001; Thomson and Ladbury 2004). Buffers containing reactive components such as reducing agents especially those with high heats of oxidation like dithiothreitol (DDT) should be avoided as they may cause artifacts in the raw data baseline. Buffers with low ionization enthalpy such as phosphate and citrate buffer are recommended as they cause few artifacts compared to those with high ionization enthalpy like Tris buffer (Pierce et al. 1999). However, in some cases, buffers with high ionization enthalpy may be used to enhance the signal strength of interactions involving protonation events (Ladbury and Doyle 2005; Perozzo et al. 2004). Matching the composition of the components in the sample cell and syringe such as concentration of salts used, pH and buffers may help to minimize dilution heat changes that may plausibly override binding signals (Freyer and Lewis 2008). Any media chosen must be of high purity and components can be dialyzed, centrifuged, or filtered to ensure no contaminants are present (Thomson and Ladbury 2004; Martinez et al. 2013). Prepared samples should also be degassed for at least 7 min using the thermovac or sonication to ensure no air bubbles are present that can interfere with the calorimetric readings.

Reproducibility of the sample preparation protocol for inorganic particles is essential for comparison between experiments. A dissolution study can be carried out to establish whether this has been achieved, whereby replicate samples containing inorganic particles as prepared for ITC experiments are dissolved in a suitable media and the ionic concentration of elements present in each quantified using inductively coupled plasma–optical emission spectroscopy (ICP-OES). The molar concentration of the nanoparticles can then be derived from its mass concentration (Huang et al. 2013).

To begin the experiment, the reference cell is filled with the solution in which the components to be studied are suspended or dissolved in hereafter referred to as the buffer. Component A is loaded into the ITC autopipette/syringe and the sample cell is filled with component B. Air bubbles that may be formed during the loading

process are expelled with the help of the loading syringe and the purging function of the control panel for the autopipette. Detailed explanation on loading of the autopipette and filling of the reference and sample cell can be found in the instrument manual and may vary depending on the instrument model and manufacturer. The syringe which has a twisted paddle on its end is then carefully placed inside the sample cell. The instrument equilibrates the temperature of the sample and the reference cell then the syringe begins to rotate and a final baseline about the chosen reference power is established. The syringe component is then periodically injected into the sample cell in predetermined aliquot volume and injection numbers.

Dilution experiments are principally conducted in order to subtract the heat changes that occur as a result of titrating the component in the syringe into the buffer. Other dilution experiments that should be considered are dilution of the buffer into the buffer and dilution of the buffer into component B in the cell which usually have negligible heat measurements (Freyer and Lewis 2008). The heat changes measured in the dilution experiment are then subtracted from the data obtained from the titration of component A into component B. The normalized heat change in kcal/mole of injectant is then plotted against the molar ratio of component A and component B. Data analysis and fitting can then be carried out using a nonlinear least-squares algorithm and suitable binding models made available by MicroCal.

The specific approach used in ITC experiments is determined by the objective of the user. For certain applications, only an accurate determination of ΔH is required and not the binding constant. Here ΔH does not need to be obtained as a fitting parameter in which case a C value greater than 100 is acceptable and the SIM can be used. If complex formation is occurring through protonation/deprotonation events, the heat signal measured may also include a contribution from buffer ionization. The experiment may, therefore, need to be performed at the same pH using buffers with different ionization enthalpies for comparison and thorough investigation of binding energetics (Cliff et al. 2004; Leavitt and Freire 2001). Where there is no buffer contributed protonation event accompanying the binding event, there will be no difference in ΔH_{obs} using the different buffers (Leavitt and Freire 2001; Perozzo et al. 2004). Different strategies are employed to measure interactions with high affinities above the upper limit of binding constants (about 10^9 M^{-1}) measurable using ITC. An example is a displacement/competition assay where the protein of interest is initially saturated with a ligand that interacts weakly before titrating with the high affinity ligand (Sigurskjold et al. 2000; Velazquez-Campoy et al. 2001). The thermodynamic linkage to temperature can also be evaluated by carrying out experiments at constant conditions and only varying the temperature within the limit of the instrument (2–80 °C). The change in heat capacity (ΔC_p) can then be determined which can be used to determine changes in hydrophobic interactions associated with binding (Cliff et al. 2004; Leavitt and Freire 2001). Standardized experimental parameters need to be applied in studies where comparisons need to be made between interactions of different ligands with the same macromolecule, i.e., mutagenesis studies to identify residues of an enzyme important for interaction with a ligand or mutants versus wild-type proteins with an inorganic material (De et al. 2007; Goobes G et al. 2007; Perozzo et al. 2004).

3.5.4 Data Analysis: Data Fitting Models Used in ITC Studies

Mathematical models are used to best fit integrated ITC data to obtain thermodynamic parameters using a curve-fitting process that applies a nonlinear regression procedure. Initial estimates of the parameters are made to generate a theoretical curve that is compared to and fit to the experiment data. This is achieved using an algorithm through an iteration process that minimizes the error function. MicroCal provides a data fitting software using Origin with three different binding models: one set of identical sites model, two sets of independent sites model, and sequential binding sites model. The relevant binding model is chosen based on information that may be known about the system being studied from other parallel studies. Where limited to no information is available, the model may be chosen based on the characteristics of the isothermal profile obtained. The main aim is to fit the data with preferably the fewest adjustable parameters which is synonymous to selecting the simplest binding model that can be used to most relevantly describe the biological, physical, or chemical process (Schmidtchen 2012). For more complicated analysis, users would need to develop their own mathematical models. The statistical significance of more complicated models with increased fitting parameters can be tested using a Monte Carlo analysis (Freyer and Lewis 2008).

From our discussion of the theory behind ITC experiments, we elaborated that the instrument operates using the heat compensation principle. For each aliquot of ligand (X) injected into the ITC cell containing a macromolecule (M), when a complex is formed (MX), there is a release or absorption of heat (Q). After subtraction of dilution heat changes, the area under each peak is equated to an interaction. Also considered is, with addition of ligand into the cell, the total volume of the mixture with the macromolecule exceeds the volume of the sample cell spilling into the tube above the sample cell. Since the instrument can only detect the heat change within the sample cell (active/working volume), equations to account for the displaced volume have been formulated to conserve the mass and correct for the measured heat change. The corrected bulk concentration of macromolecule and ligand is, therefore, expressed as M_t and X_t, respectively. The mass balance expression and equilibrium constant for the three models used by MicroCal® ITC Origin™ are as follows:

(i) One set of identical sites model: Applied where all binding sites have the same ΔH and K values

$$K = \frac{\Theta}{(1 - \Theta)[X]} \tag{3.6}$$

where 1 represents total number of binding sites of the macromolecule available and unoccupied (unbound macromolecule), Θ represents the fraction of sites that are occupied by ligand X and the concentration of free/unbound ligand is represented as $[X]$. From this binding model, the output gives one value for n, K, ΔH, and ΔS.

(ii) Two sets of independent sites model: For independent interactions where macromolecules have two different binding sites with separate values of K and ΔH. Therefore, two values are obtained for each parameter n, K, ΔH, and ΔS relating to the first and the second binding site.

$$K_1 = \frac{\Theta_1}{(1-\Theta_1)[X]} \quad \text{and} \quad K_2 = \frac{\Theta_2}{(1-\Theta_2)[X]} \tag{3.7}$$

Each binding site being independent means that where $n1 = 1$ and $n2 = 2$, one ligand binds to the first site and two ligands of equivalent thermodynamics bind to the second site. For interactions that have independent binding sites, n being a nonintegral value is an indicator of errors to do with concentration (Freyer and Lewis 2008). The equilibrium constant is in actuality defined from the activities of interacting species rather than their concentration therefore errors in determination of concentration could arise especially when working with larger macromolecules like proteins which could be pure but not correctly folded hence inactive (Ball and Maechling 2009).

(iii) Sequential binding sites model: Used where an interaction at one binding site influences a subsequent interaction at another binding site (negative or positive cooperativity). In this model, the binding sites could be identical or nonidentical and there is no clear distinction as to which specific binding sites are saturated. Only the total number of saturated binding sites can be known thus the binding constant is defined relative to the evolution of saturation. For interactions that are dependent, the n value is excluded as a fitting parameter because nonintegral values of no physical sense would be obtained. Unique parameters for K, ΔH, and ΔS are obtained for each number of sites which is determined by the user.

$$K_1 = \frac{[MX]}{[M][X]}, \quad K_2 = \frac{[MX_2]}{[MX][X]} \quad \text{and} \quad K_3 = \frac{[MX_3]}{[MX_2][X]} \tag{3.8}$$

Detailed descriptions of the mathematical formulae corresponding to ITC models have been elaborated in the instrument user manual provided by MicroCal and in the literature (Chilom et al. 2004; Martinez et al. 2013; Perozzo et al. 2004; Poon 2010). In the following section, we will further describe how thermodynamic parameters can be determined using the simplest model, one set of identical sites model and later discuss how the model can be modified to more suitably portray peptide–inorganic interactions using proposed changes discussed in the section on the literature studies (Goobes G et al. 2007).

3.5.5 Determination of Thermodynamic Parameters Using One Set of Identical Sites Model

The equilibrium constant (K) and the total ligand concentration (X_t) can be expressed using the following equations;

$$K = \frac{\Theta}{(1-\Theta)[X]} \tag{3.9}$$

$$X_t = [X] + n\Theta M_t \tag{3.10}$$

Combining Eqs. (3.9) and (3.10) gives a quadratic equation that is solved as follows:

$$K = \frac{\Theta}{(1-\Theta)[X_t - n\Theta M_t]} \tag{3.11}$$

$$\Theta^2 - \Theta\left(1 + \frac{X_t}{nM_t} + \frac{1}{nKM_t}\right) + \frac{X_t}{nM_t} = 0 \tag{3.12}$$

$$\Theta = \frac{-\left(1 + \frac{X_t}{nM_t} + \frac{1}{nKM_t}\right) \pm \sqrt{\left(1 + \frac{X_t}{nM_t} + \frac{1}{nKM_t}\right)^2 - \frac{4X_t}{nM_t}}}{2} \tag{3.13}$$

The total heat content (Q) in the sample cell is proportional to the number of binding sites (n), the fraction of the sites that have been occupied by the ligand (Θ), the molar heat of binding for the ligand (ΔH), and the total macromolecule concentration (M_t) in the volume of the sample cell where the heat change is detectable (V_o).

$$Q = n\Theta M_t \Delta H V_O \tag{3.14}$$

Substituting Θ into the above equation gives

$$Q = \frac{nM_t\Delta HV_O}{2}\left[1 + \frac{X_t}{nM_t} + \frac{1}{nKM_t} - \sqrt{\left(1 + \frac{X_t}{nM_t} + \frac{1}{nKM_t}\right)^2 - \frac{4X_t}{nM_t}}\right] \tag{3.15}$$

The heat change of each injection, ΔQ (i) taking into account correction of displaced volume can be expressed as

$$\Delta Q(i) = Q(i) + \frac{dV_i}{V_o}\left(\frac{Q(i) + Q(i-1)}{2}\right) + Q(i-1) \tag{3.16}$$

3.5.6 Case Studies on the Use of ITC in Materials Science

Applications of ITC have evolved from conventional biomolecular recognition reactions into diverse areas of interest in both academic and industrial laboratories. The exploration into novel systems equally drives the development and improvement of experiment strategies and data analysis. ITC protocols are developing in other fields including drug design, polymer chemistry, and nanotechnology hence studies where ITC has been successfully used to probe interactions between different ligand molecules with inorganic/organic materials continue to emerge. Some of these studies and research directions mainly involving interactions with suspensions of metals and metal oxide particles as well as metal ions have been highlighted in this chapter to provide a snapshot of the evolving applications of ITC in materials science and particularly interactions at the biotic–abiotic interface.

Among the pioneering studies applying ITC to investigate ligand–nanoparticle interactions was a study to characterize interactions between amino acids and the surface of gold nanoparticles (Joshi et al. 2004). Gold nanoparticles can be modified and functionalized through binding of specific ligands, i.e., thiols and amine groups (Jana et al. 2001; Kumar et al. 2003). Joshi et al. (2004) specifically endeavored to use ITC to investigate the interactions between gold nanoparticles with a basic (lysine) and an acidic (aspartic acid) amino acid. They observed that amine groups bind strongly with gold nanoparticles in their unprotonated state (Joshi et al. 2004). At physiological pH, lysine was found to interact weakly with gold nanoparticles compared to aspartic acid. This was thought to occur because at pH 7, amine groups in lysine (pI 9.4) may have been protonated while the amine groups of aspartic acid (pI 2.77) remained unprotonated (Joshi et al. 2004). When the experiments were repeated at pH 11, the amine group of lysine could interact more strongly with gold nanoparticles as they were unprotonated (Joshi et al. 2004). From TEM studies of nanoparticles used in the ITC experiments, the authors observed variable degrees of particle aggregation and concluded that accurate reproducibility of the surface area available for interaction with amino acids between experiments could not be attained.

In a similar study, ITC was used to characterize the energetics of interaction of deoxyribonucleic acid (DNA) and peptide nucleic acids (PNA) base monomers with gold nanoparticles (Gourishankar et al. 2004). Their aim was to design oligonucleotides that can complex with gold nanoparticles based on their different binding strengths without the need of thiolation. Gold nanoparticles modified using DNA and PNAs are of interest for applications such as sensors, biodiagnostics, chips, imaging, drug/DNA delivery, and structured nanoparticle assemblies with electronic properties (Gourishankar et al. 2004). In another study, surface modified gold nanoparticles were used to template the growth of hydroxyapatite crystals which are of interest for biomedical applications (Rautaray et al. 2005). Here, ITC was used to characterize interactions between gold nanoparticles capped with aspartic acid which can bind to calcium ions and induce crystal growth. In this

study, the authors also concluded that it was not possible to accurately determine the concentration of aspartic acid bound to gold nanoparticles as the total surface area of the gold nanoparticles could only be estimated (Rautaray et al. 2005). In all the above mentioned studies, binding isotherms were plotted against the total volume of the component injected into the cell instead of the molar ratio of interacting components; thus thermodynamic parameters of the interactions were not determined. However, the nature of the interaction and qualitative trends in the binding behavior of the amino acids could be identified (Gourishankar et al. 2004; Joshi et al. 2004, Rautaray et al. 2005). From the above studies, ITC showed great potential in its use to monitor the interactions between ligands and nanoparticles and the development of its application into new fields was encouraged.

ITC has been used in the advancement of novel hybrid materials that can specifically target a protein–protein interaction that would otherwise not occur in nature but could have beneficial applications (De et al. 2007; You et al. 2008). Artificial protein receptors can be created using nanoparticles whose surface can be modified to become surface receptors that can be recognized by proteins (De et al. 2007; You et al. 2008). ITC was successfully used to determine the selectivity and binding thermodynamics of the interactions between gold nanoparticles functionalized with amino acids/dipeptides (bearing leucine and/or phenylalanine residues) and target proteins; cytochrome *c* (CytC) and α-chymotrypsin (ChT) (You et al. 2008). Because the nanoparticles were functionalized, the interaction is essentially a peptide–protein interaction but may be distinctively different from the mechanism through which the free amino acid/dipeptide interacts with the protein. This study has been specifically highlighted to illustrate how circular dichroism (CD) can be used to determine the arrangement of dipeptides and amino acids on the surface of gold nanoparticles (Huang et al. 2013; You et al. 2008). This approach can similarly be transferred to aid interpretation of thermodynamic data where direct interactions of molecules, i.e., peptides with nanoparticles is conducted. By determining the density of surface coverage using CD one may be able to deduce whether the adsorbed molecules form monolayers or multilayers through ligand–ligand self-recognition interactions. In this study, from CD analysis, no significant interaction between adjacent amino acid/dipeptide functionalities was detected which could otherwise occur through hydrogen bonding (You et al. 2008). For the enantiomeric dipeptides used to functionalize the gold nanoparticles, mirror CD signals suggested equal load on particles and ca. 100 amino acids were estimated to be bound to each nanoparticle. The concentration of nanoparticles was determined based on their average molecular weights considering the gold core's size dispersion. Heat change was measured for the complexation of ChT and CytC with the functionalized nanoparticles (Fig. 3.13).

Data obtained was fit using a single set of identical sites model for the interaction with ChT based on the sigmoid shape of the curve obtained and the interaction with CytC was fit using both the single set of identical sites and two sets of independent sites model (Table 3.4). A compensatory relationship was observed between enthalpy and entropy during the complexation process. The authors state that the bimodal binding observed with CytC is unknown but may

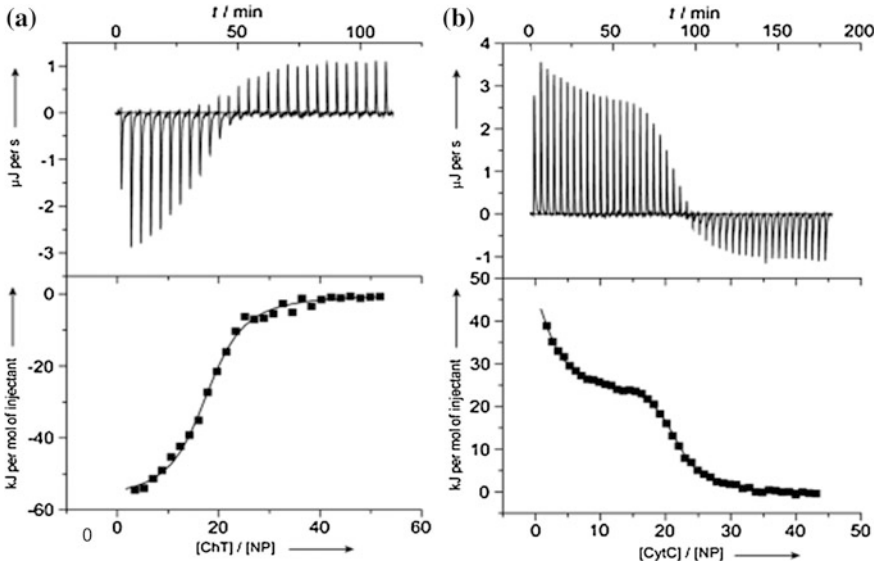

Fig. 3.13 ITC isotherms showing the heat changes measured during the interaction of **a** ChT with gold nanoparticles functionalized with a dipeptide L-phenylalanine- D phenylalanine fit using one set of identical sites model **b** CytC with gold nanoparticles functionalized with dipeptide L-leucine-L-leucine fit using two sets of independent sites model. Experiments were conducted in sodium phosphate buffer pH 7.4. Reprinted with permission from You et al. (2008) John Wiley and Sons

arise from the particle's potential anisotropicity or through possible variations in the binding geometry of CytC via protein–protein interactions (You et al. 2008). They proposed that complexation may occur through hydrophobic interactions and charge complementary interaction. They also highlighted the effect of amino acid/dipeptide chirality on complex stability. They concluded that with further investigation, knowledge gained could be used to manipulate protein recognition, specificity, affinity, and stability of the interactions formed paving the way for advances in creation of novel hybrid materials (You et al. 2008).

Another study of hybrid materials that employed ITC was conducted by Chiad et al. (2009) in which surface modification of SiO_2 via interaction with amphiphilic monomers and copolymers was investigated. The formation of these organic–inorganic hybrid systems occur through noncovalent adsorption of amphiphilic compounds to the surface of inorganic particles and the strength and irreversibility of the interaction is of great interest (Chiad et al. 2009; Hoffmann et al. 2006). The amphiphilic compounds used were monomers, i.e., 2-ethylhexyl methacrylate (EHMA), poly(ethylene oxide) methacrylate having 5 (PEOMA$^{n \approx 5}$), and 9(PEOMA$^{n \approx 9}$) ethylene oxide units, poly(propylene oxide) methacrylate (PPOMA), 2-hydroxythyl methacrylate (HEMA) (ethyl glycol) methacrylate phosphate (EGMP), 4-viny-1-(3-sulforopyl)pyridinium inner salt

Table 3.4 Thermodynamic parameters (in kJ mol^{-1}), dissociation constants (K_D), and binding stoichiometry (n) obtained through ITC measurements of the interaction between ChT and CytC with functionalized gold nanoparticles in phosphate buffer pH 7.4 at 30 °C

Protein	Nanoparticle[b]	First binding event						Second binding event			
		K_D^1[μM]	ΔG	ΔH	$T\Delta S$	n	K_D^2[μM]	ΔG	ΔH	$T\Delta S$	n
	NP_Gly-Gly	2.14 ± 0.20	−32.9	-37.1 ± 1.9	−4.2	11.6	–				
	NP_L-Leu	2.45 ± 0.34	−32.6	-46.6 ± 25	−14.0	8.8	–				
	NP_D-Leu	138 ± 0.07	−34.0	-47.0 ± 03	−13.0	9.2	–				
	NP_L-Phe	229 ± 0.05	−32.7	−54.9 ± 2-8	−22.2	13.2	–				
	NP_D-Phe	1.12 ± 0.16	−34.5	−59.3 ± 0.9	−24.7	17.2	–				
ChT[a]	NP_L-Leu-L-Leu	132 ± 0.12	−34.1	−36.0 ± 0.6	−1.9	15.2	–				
	NP_L-Leu-D-Leu	1.05 ± 0.12	−34.7	−47.6 ± 1.6	−12.9	12.8	–				
	NP_L-Leu-L-Phe	0.81 ± 0.02	−35.3	−56.0 ± 1.0	−20.7	18.0	–				
	NP_L-Leu-D-Phe	058 ± 0.05	−36.2	−49.1 ± 05	−12.9	20.0	–				
	NP_L-Phe-D-Phe	0.82 ± 0.07	−35.3	−55.1 ± 1.6	−19.8	17.0	–				
	NP_D-Phe-L-Phe	1.17 ± 0.15	−34.5	−46.9 ± 3.6	−12.4	11.2	–				
	NP_D-Phe-D-Phe	0.44 ± 0.05	−36.9	−44.4 ± 13	−7.6	22.8	–				
	NP_Gly-Gly	0.023 ± 0.004	−44.3	12.3 ± 2.0	56.6	1.8	1.78 ± 0.34	−33.4	4.9 ± 1.2	38.2	13.6
	NP_L-Leu	0.251 ± 0.012	−38.3	189.6 ± 3.0	227.9	2.0	1.95 ± 0.09	−33.1	2.3 ± 0.2	35.4	18.2
	NP_D-Le u	0.044 ± 0.008	−42.7	116.0 ± 0.1	158.5	1.6	1.12 ± 0.31	−34.5	6.6 ± 0.6	41.2	11.8
	NP_L-Phe	0.068 ± 0.006	−41.6	28.8 ± 0.1	70.4	2.2	1.51 ± 0.21	−33.8	13.1 ± 1.0	46.9	9.6
	NP_D-Phe	0.015 ± 0.005	−45.5	55.0 ± 45	100.6	2.6	3.02 ± 0.98	−32.0	13.8 ± 0.5	45.8	14.6
	NP_L-Leu-L-Leu	0.107 ± 0.015	−40.4	59.1 ± 1.6	99.5	2.2	1.29 ± 0.42	−34.2	25.5 ± 0.8	59.7	19.4
CytC	NP_L-Leu-D-Leu	0.692 ± 0.034	−35.7	31.4 ± 1.6	67.2	1.8	1.74 ± 0.24	−33.4	21.7 ± 0.2	55.2	13.6
	NP_L-Leu-L-Phe	0.025 ± 0.003	−44.2	34.8 ± 0.7	78.9	2.9	1.62 ± 0.22	−33.6	24.6 ± 0.9	58.2	10.6
	NP_L-Leu-D-Phe	0.525 ± 0.097	−36.4	34.9 ± 0.7	71.4	2.0	1.48 ± 0.41	−33.8	21.2 ± 0.2	55.1	23.6
	NP_L-Phe-D-Phe	0.251 ± 0.077	−38.3	49.2 ± 32	87.6	2.2	0.98 ± 0.23	−34.9	25.7 ± 1.7	60.6	15.8
	NP_D-P he- L-Phe	0.245 ± 0.114	−38.4	40.7 ± 4.7	79.1	1.8	1.00 ± 0.28	−34.8	21.2 ± 0.2	56.0	18.6
	NP_D-Phe-D-Phe	0.022 ± 0.004	−44.4	36.0 ± 2.6	80.3	2.6	0.79 ± 0.26	−35.4	21.7 ± 0.3	57.1	15.0

Reprinted with permission from You et al. (2008) John Wiley and Sons

a Refers to the differences between binding constants determined using ITC and those previously determined using enzyme activity assays (You et al. 2005a, You et al. 2005b) which may have been due to differences in experiments conditions.

b The concentration of nanoparticles in ITC experiments was determined as an average of molecular weights taking into consideration the size dispersion of gold cores. This was different from previous determination of NP concentration using UV absorbance hence the differences in binding stoichiometries obtained.

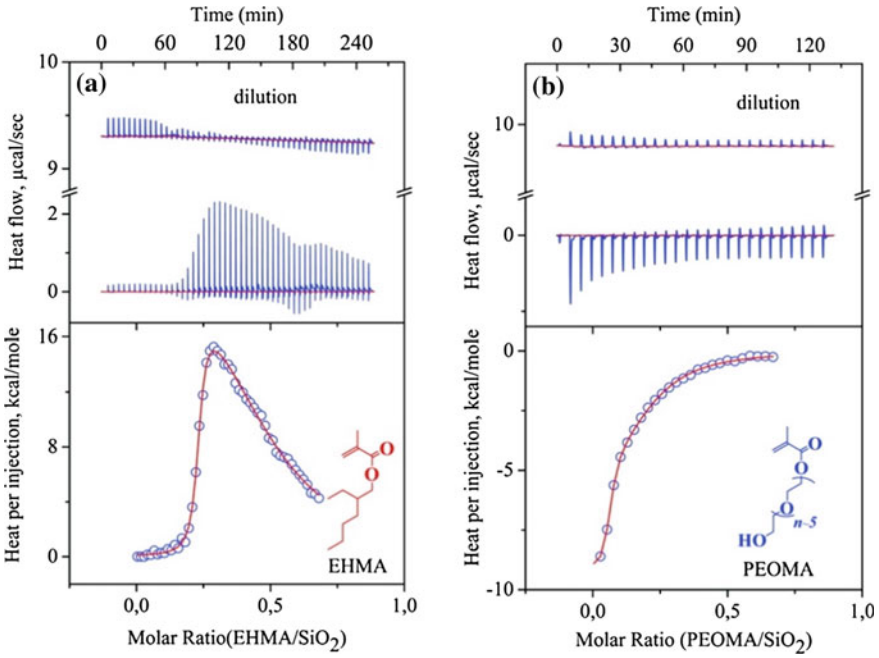

Fig. 3.14 ITC isotherms showing the titration of **a** hydrophobic monomer EHMA and **b** hydrophilic PEOMA$^{n \approx 5}$ into a suspension of SiO_2 in the chosen solvent mixture 1,4-dioxane/ethanol/H_2O. Reprinted with permission from Chiad et al. (2009) American Chemical Society

(4VPSB), and copolymers PEHMA-*co*-PEGMP, PEHMA-*co*-PPEOMA$^{n \approx 5}$, and PEHMA-*co*-P4VPSB. The titration of hydrophobic EHMA and hydrophilic PEOMA$^{n \approx 5}$ into suspensions of SiO_2 nanoparticles are shown in Fig. 3.14.

The Thermodynamic parameters of interaction (ΔH, ΔS, K_B, and ΔG) were determined (Table 3.2). The authors inferred that the low ΔH value obtained in the titration of EHMA with SiO_2 indicates that there was no significant interaction of the polymer with the surface. They also attributed the observed endothermic heat changes to the collapse of the structure of water molecules surrounding the hydrophobic EHMA molecules. An enthalpically driven interaction was registered in the interaction of hydrophilic PEOMA with SiO_2 that was attributed to possible hydrogen bonding or van der Waals interactions. The authors stated that changes in conformational entropy of PEOMA and solvation entropy could also have occurred during the adsorption reflected by ΔS values (Table 3.5). In conclusion, they stated that the approach of studying the thermodynamic changes occurring at interfaces could possibly allow one to directly correlate adsorption strength to the structure of inorganic particles allowing materials engineering to be conducted using more rational and optimized methods (Chiad et al. 2009).

Table 3.5 Thermodynamic parameters of the interaction of amphiphilic monomers and copolymers with SiO_2 nanoparticles determined using ITC

Surface-active compound	K_B (mol L^{-1})	ΔH (kcal mol^{-1})	TΔS (kcal mol^{-1})	ΔG (kcal mol^{-1})
EHIB[a]	$1.10 \times 10^7 \pm 4.30 \times 10^6$	0.25 ± 0.18	10.19	−9.94
	$1.00 \times 10^5 \pm 1.50 \times 10^4$	63.46 ± 2.70	70.36	−6.88
PEOIB[a]	$3.87 \times 10^4 \pm 1.33 \times 10^4$	-13.60 ± 9.99	−7.33	−6.25
EHMA[a]	$1.90 \times 10^7 \pm 3.00 \times 10^6$	0.04 ± 0.01	9.98	−9.94
	$5.70 \times 10^4 \pm 6.20 \times 10^3$	25.50 ± 1.43	31.90	−6.40
PEOMA$^{n \approx 5}$[a]	$6.10 \times 10^4 \pm 6.50 \times 10^3$	-25.13 ± 4.23	−18.60	−6.53
HEMA[b]	$8.26 \times 10^4 \pm 2.27 \times 10^4$	-0.19 ± 0.04	6.49	−8.20
PEOMA$^{n \approx 5}$[b]	$6.35 \times 10^3 \pm 0.04 \times 10^3$	-43.50 ± 0.20	−38.16	−5.34
PEOMA$^{n \approx 9}$[b]	$1.15 \times 10^5 \pm 2.03 \times 10^4$	-69.87 ± 0.54	−62.90	−6.97
PEOMA$^{n \approx 5}$[b]	$1.5S \times 10^5 \pm 0.92 \times 10^4$	-0.05 ± 0.007	7.04	−6.98
4VPSB[a]	$1.74 \times 10 = \pm 3.05 \times 10^4$	-27.57 ± 2.24	−20.42	−7.14
EGMP[a]	$4.33 \times 10^4 \pm 2.35 \times 10^3$	-39.85 ± 0.8	−33.39	−6.46
PEHM A-*co*-PPEOMA$^{n \approx 5}$	$2.50 \times 10^5 \pm 4.40 \times 10^4$	-10.01 ± 0.53	−2.77	−7.33
PEHMA-*co*-P4VPSB	$5.70 \times 10^5 \pm 3.29 \times 10^5$	-8.77 ± 0.20	−0.92	−7.86
PEHM A-*co*-PEGMP	$4.78 \times 10^5 \pm 0.00$	-10.26 ± 0.16	−2.51	−7.75

Reprinted with permission from Chiad et al. (2009) American Chemical Society
[a] Concentration of the hydrophilic monomer = 55 mM
[b] Concentration of the hydrophilic monomer = 278 mM

In biomineralization studies, ITC has been used to study the thermodynamics of biomolecule interactions with biominerals. Statherin is an oral cavity protein that regulates the nucleation and growth of hydroxyapatite (HAP) and serves as a receptor for bacterial adhesion to enamel. Extensive studies on the interaction of statherin to HAP have been carried out to identify the underlying molecular mechanisms (Goobes R et al. 2007; Raj et al. 1992; Wikiel et al. 1994). The wild-type sequence of statherin consists of 43 amino acid residues. The first five residues are negatively charged and have been identified to directly participate in binding to hydroxyapatite (Goobes R et al. 2007; Raj et al. 1992; Wikiel et al. 1994). The acidic amino acids are followed by a basic amino acid rich segment whose role was unknown. The roles of the positively charged residues were determined by carrying out single and multiple point mutations replacing the basic residues with alanine amino acid (Goobes R et al. 2007). The interaction of the wild-type and mutant protein with HAP crystals was then studied using ITC and equilibrium adsorption binding isotherms (AI) as shown in Table 3.6 (Goobes R et al. 2007). Synthesized proteins were all labeled at specific positions for studies on the structure of the adsorbed protein using solid-state NMR rotational echo double resonance (ss-NMR REDOR) and dynamics measurements (Goobes R et al. 2007).

To attain the above thermodynamic parameters, Goobes R et al. (2007) proposed that when studying peptide–inorganic interactions, the equilibrium constant

Table 3.6 Thermodynamic parameters of the interaction of statherin and its mutants with HAP determined using equilibrium adsorption isotherms and ITC

Protein	N_{max} (10^{-7} mol/m^2)	K (10^{5}/M)	ΔG^0(kcal/mol)	$\Delta\Delta G^0$ (kcal/mol)	$\Delta H^b_{initial}$ (kcal/mol adsorbed)
stalh (WT)	6.2 ± 0.7	7.0 ± 0.9	−7.9 ± 0.]		−3.3 ± 0.4, 90 %
stathik6Al	7.3 ± 0.9	2.8 ± 0.6	−7.4 ± 0.]	0.5 ± 0.1	−3.7 ± 0.5, 85 %
stath (R9A)	6.8 ± 0.3	2.8 ± 0.5	−7.4 ± 0.1	0.5 ± 0.1	−3.2 ± 0.3, 85 %
stath (RlOA)	5.7 ± 0.8	4.5 ± 1.2	−7.6 ± 0.2	0.3 ± 0.2	−3.8 ± 0.4, 85 %
stath (R 13 A)	6.4 ± 0.8	4.0 ± 1.0	−7.6 ± 0.2	0.3 ± 0.2	−3.1 ± 0.3, 85 %
stath (KRA)	3.0 ± 1.2	1.5 ± 0.8	−7.0 ± 0.3	0.9 ± 0.3	−3.7 ± 0.4, 45 %

N_{max}, K, $\Delta G°$ and $\Delta\Delta G°$ were determined from AI measurements and from ITC experiments, $\Delta H_{initial}$ was determined which was the initial enthalpy change which corresponded to direct protein interaction with the surfaces of HAP. Experiments were conducted in phosphate buffer pH 7.4 at 25 °C. Reprinted with permission from Goobes R et al. (2007) American Chemical Society

(K) and the total ligand concentration (X_t) can be expressed as previously described in the section on data analysis but M_t should be redefined. M_t can be modified to express the surface area of the inorganic particle which is the binding site as the effective concentration of sites on the surface ($\boldsymbol{M_t'}$) that are available for interaction with the peptide using the following expression;

$$M_t' = N_{max}\left(\frac{\text{moles}}{m^2}\right) \times \text{SA}\left(\frac{m^2}{\text{gr}}\right) \times D\left(\frac{\text{gr}}{L}\right) \tag{3.17}$$

Equilibrium adsorption isotherm measurements (AI) can be used to quantify the maximum number of peptide interaction sites (N_{max}) per unit surface area of the inorganic particle. In AI measurements if centrifugation is used to separate the supernatant with free protein from the pellet-containing particles with adsorbed peptide, this may perturb the peptide–nanoparticle complex leading to inaccurate quantification of bound and free peptide (Klein et al. 2007). The total surface area (SA) of the inorganic particles can be determined from BET measurements although there may be discrepancies between the surface sites that are accessible to small gaseous molecules such as nitrogen used in BET experiments compared to the size of interacting molecules being studied (Goobes R et al. 2007). The density (D) of the inorganic particles in the ITC cell is obtained by dividing its mass by the volume of the cell (Goobes R et al. 2007).

The binding affinity of the single point mutant protein to the surfaces of HAP was lowered compared to the wild-type protein but the adsorption enthalpy, dynamic properties, structural properties, and the maximal surface coverage was not altered. The multiple point mutation of the wild-type protein replacing all basic residues with alanine simultaneously resulted in a fivefold reduction of the binding constant and a twofold reduction of the surface coverage despite no observed changes in the structure and dynamics of the *N*-terminal acidic segment. They deduced that the surface coverage of the multiple point mutant may have been

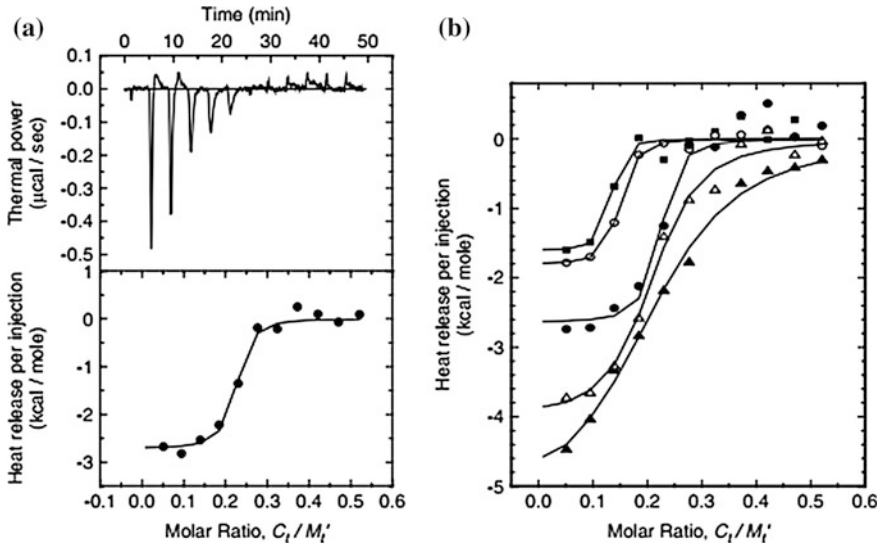

Fig. 3.15 ITC profiles of the interaction of statherin with HAP **a** experiment conducted at 25 °C **b** experiment carried out at different temperatures, i.e., 15 °C (*black triangle*), 20 °C (*white triangle*), 25 °C (*black circle*), and 30 °C (*white circle*), 37 °C (*black square*). Reprinted with permission from Goobes G et al. (2007) John Wiley and Sons

decreased due to unfavored protein–protein interaction as a result of stronger repulsive charge between the higher negative net charge compared to the wild-type protein and single point mutants. In consistency with their previous studies, the authors proposed two binding sites for statherin on HAP surface; the first eliciting an exothermic heat change that can be correlated to statherin interacting with the crystal faces and step edges of HAP and the second that does not cause a measurable heat change and can be attributed to release of bound water and protein–protein interaction. The second binding site is therefore best characterized using binding models based on determination of surface coverage which can give a clearer indication of the occurrence of protein–protein interaction. For the measurable heat change in the initial interaction, all mutants and the wild-type possessed comparable binding entropy when studied using ITC. Any possible changes in enthalpy of the mutants compared to the wild-type may have been below the detection limit of the ITC instrument used. For the second interaction, the enthalpy contribution may be canceled by other events or may also be below the ITC's detection limit. The authors concluded that the basic amino acids do not significantly contribute to the protein's enthalpy of adsorption but influence the packing density of the protein at saturation (Goobes R et al. 2007).

In another study, statherin was titrated into a suspension of HAP crystals in a calorimetry cell at different temperature between 15 and 37 °C (Goobes G et al. 2007). The integrated heat change was plotted against the ratio of total protein concentration (C_t) after each injection and the effective concentration of binding

Table 3.7 Thermodynamic parameters of the interaction of statherin with HAP in phosphate buffer pH 7.4 determined using ITC

Temp (°C)	α	ΔH (kcal/mole)	$T\Delta S^0$ (kcal/mole)	ΔG^0 (kcal/mole)	K (1/M)
15	0.21	-5.4 ± 0.4	2.1 ± 0.3	-7.4 ± 0.1	$(4.3 \pm 0.8) \times 10^5$
20	0.18	-4.0 ± 0.4	4.1 ± 0.2	-8.1 ± 0.2	$(1.1 \pm 0.4) \times 10^6$
25	0.21	-2.7 ± 0.1	6.8 ± 0.2	-9.5 ± 0.4	$(9.5 \pm 5.8) \times 10^6$
30	0.13	-1.8 ± 0.2	8.0 ± 0.2	-9.8 ± 0.3	$(1.2 \pm 0.6) \times 10^7$
37	0.11	-1.6 ± 0.4	6.5 ± 0.3	-10.1 ± 0.5	$(1.4 \pm 1.0) \times 10^7$

Only a fraction of the interactions that occur elicit a measurable heat change by ITC and are represented by α. Reprinted with permission from Goobes G et al. (2007) John Wiley and Sons

sites on the HAP surface (M'_t) available for statherin adsorption (Fig. 3.15). As in the previous study, adsorption occurred through an initial exothermic event followed by a thermoneutral event. The apparent thermodynamic parameters of the interactions are shown in Table 3.7. The exothermic event was seen to decrease with an increase in temperature. The determined ΔCp and ΔS of the interaction were positive and collectively suggest that electrostatic and not hydrophobic interactions dominated the interaction likely through the charge interactions of ionic HAP surface sites and the charged N-terminus of the protein (Goobes G et al. 2007).

The bottom-up hierarchical approach to material assembly using biomolecules to control growth and morphology of materials is increasingly applied with an aim of achieving programmable structures with superior functions. In our studies, we have applied ITC to study the interaction of ZnO-twinned hexagonal rods and synthetic inorganic binding peptides that have been shown to modify the morphology of the inorganic materials during synthesis studies in the presence and absence of the peptides (Liang et al. 2011; Tomczak et al. 2009). Data showing the interaction of GT-16 peptide (GLHVMHKVAPPR-GGGC) with ZnO crystals has been illustrated in Fig. 3.12a. We have also studied the interaction of ZnO with G-12 peptide (GLHVMHKVAPPR) and its alanine mutants using computational tools (Tripos SYBYL and Accelyrys Materials studio) and ITC. Additionally, we have carried out synthesis of ZnO in the presence of wild-type G-12 peptide and some selected mutants. Interaction studies using peptide G-12 (GLHVMHKVAPPR) with uncalcined and calcined crystals show differences in the isothermal profiles highlighting the importance of surface characterization (Fig. 3.16).

In addition, for binding experiments conducted with single point mutants of G-12, differences in the features of the isothermal profiles can be observed (Fig. 3.17). From the ITC data, there is a clear participation of two interaction process of opposite heat change; an endothermic event followed by an exothermic event. The observed endothermic interaction may reflect changes in peptide conformational entropy influenced by the intrinsic properties of the peptide and by the structuring effect of water molecules. Endothermic interactions measured could also have resulted from displacement of water molecules that interact with the surface of ZnO thereby breaking hydrogen bonds before the peptide interacts. This may be the reason why less of the endothermic event is seen for the calcined

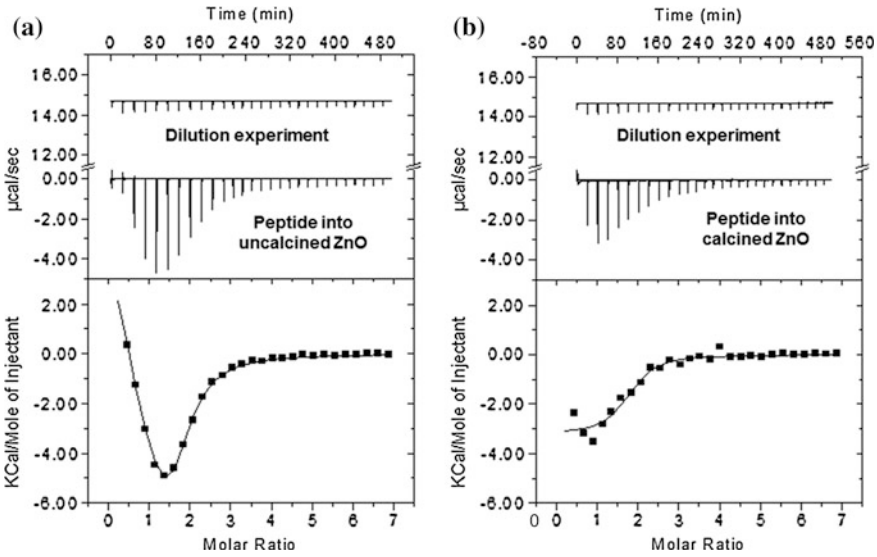

Fig. 3.16 ITC isotherms representing the interaction of as prepared (uncalcined) ZnO rods and calcined ZnO rods with G-12 peptide. **a** *Above*, raw data profile of titrating 280 µl of 3.125 mM G-12 peptide in 10 µl aliquots into a cell containing 1.4 ml of ddH_2O producing heats of dilution. *Below* is the raw data profile of titrating the peptide into a cell containing a suspension of 0.1 mM ZnO rods. **b** A similar experiment of G-12 interaction with calcined ZnO hexagonal crystal rods (Unpublished data)

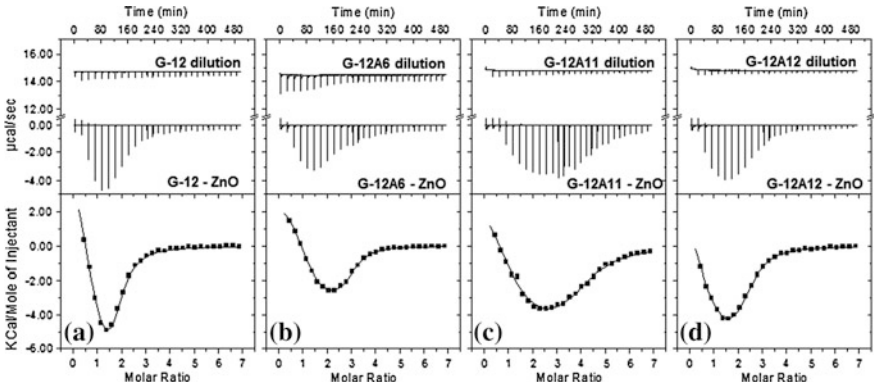

Fig. 3.17 ITC isotherms showing interaction of G-12 peptide and mutants with ZnO rods. **a** G-12 peptide, **b** G-12A6 peptide, **c** G-12A11 peptide, **d** G-12A12 peptide. In all experiments, 3.125 mM peptide was added in 28 injections each with 10 µl aliquots into a cell containing 1.4 ml ZnO rods suspension containing 0.1 mM Zn^{2+}. A constant cell temperature of 298 K was maintained (unpublished data)

ZnO crystals. Exothermic heat changes observed may be as a result of the interaction occurring between the peptide and the inorganic surface via noncovalent interactions such as van der Waals interaction, electrostatic interactions, or hydrogen bonding.

Quantification of binding potency can be based on the amount of material that adsorbs to the surface. The amount of peptide needed to obtain saturation in all the interactions was found to be in excess of the amount required to form a monolayer of peptide on the surface of ZnO available. This may suggest that the peptides could have self-recognition properties allowing them to bind to each other thus forming multilayers on the surface of ZnO. Two saturation events could be taking place: peptide binding and saturating the surface of ZnO and peptide binding to peptide forming a multilayer until peptide–peptide binding site saturation is achieved. Each event produces a measurable heat change; however, there is no clear distinction between the saturation of the peptide layer directly adsorbing onto the inorganic surface and subsequent saturation of the peptide–peptide interaction events. It is likely that both events would occur simultaneously rather than sequentially as the peptides could have adsorbed in an aggregated form as evidenced from DLS experiments showing that peptides are polydisperse and aggregated in solution. From synthesis studies in the absence and presence of G-12 peptide and mutant peptides, structural modification was also found to be peptide dependent.

Nanoparticles are increasingly being developed and administered in products including medicine (Lindman et al. 2007; Lynch and Dawson 2008; Mahmoudi et al. 2011). They are of interest mainly because of their small size which enhances their chemical reactivity through increasing the number of surface atoms and in biomedical applications, allows them to infiltrate into target sites that were previously inaccessible as well as to interact more intimately with cellular machinery. Nevertheless, reservations on their use linger as there is insufficient knowledge on the biological responses they elicit including toxicity which is alarming. In biological fluids, nanoparticles are coated with proteins forming the nanoparticle–protein corona which is the entity that the cells recognize and interact with (Lindman et al. 2007; Lynch and Dawson 2008). Studying the plausible toxicological effects of nanoparticles requires a detailed account of its interaction with proteins to determine which proteins enrich the nanoparticle surface. ITC has been used to determine the thermodynamics of interaction of human serum albumin (HSA) to copolymer nanoparticles or varying sizes/curvature and hydrophobicity (Lindman et al. 2007). Exothermic events were registered for all the nanoparticles used and the more hydrophobic nanoparticles required a higher concentration of HSA to be saturated which the authors inferred to suggest a higher surface coverage. Higher affinity was observed for the more hydrophilic nanoparticles. MOLMOL which is a molecular graphics program was used to calculate the maximum number of protein molecules that adsorb to the nanoparticle by estimating the minimum cross-section area of HSA structure. The theoretical surface area of the particles were also calculated and divided by the cross-sectional area of HSA achieving theoretical 100 % coverage for each particle. The sparse or dense

nature of the adsorbed protein layer (monolayer or multilayers) can be determined from the degree of surface coverage (Lindman et al. 2007). The surface coverage of nanoparticles with the same hydrophobicity but different particle size was also investigated. The curvature of the nanoparticles was seen to affect surface coverage (Cedervall et al. 2007; Lindman et al. 2007). The smallest nanoparticles (70 nm) with the highest available surface area for interaction were found to have less bound protein which was attributed to the high degree of curvature which could have interfered with binding. The larger nanoparticles (700 nm) tended toward a flat surface hence the effect of surface curvature became more insignificant. Particles between 120 and 400 nm had the highest surface coverage. A dense adsorbed layer of protein was observed for nanoparticles of 120 nm diameters and larger. However, the shape of the isothermal profiles did not suggest the occurrence of multilayers normally represented by steps as each layer is completed. This was attributed to undetectable entropy changes of protein–protein interactions similar to previous reports on the interaction of statherin with HAP (Goobes R et al. 2007, Lindman et al. 2007). Possibly as in the previously discussed study by You et al. (2008), CD measurements could be used to confirm if multilayer formation occurred. The authors also studied the interaction of other proteins including lyzozyme, fibrinogen, and calmodulin with copolymer nanoparticles using ITC but no signals were found (Lindman et al. 2007). They concluded that the lack of signals could be as a result of no measurable heat change of interactions if reactions were entirely entropy driven or because there was no interaction. SPR was used as a complementary technique which confirmed that interactions could not be ruled out with some of the studied proteins which were contrarily found to interact with the copolymer nanoparticles that were immobilized to a gold surface using a thiol group. This underlines the benefits of using complementary techniques (Lindman et al. 2007).

Lindman et al. (2007) further studied the interaction of nanoparticles with HSA bound to its endogenous ligand oleic acid. The interaction was endothermic which they thought could have resulted from initial dissociation of oleic acid from HSA before it binds to the nanoparticle or variations in the binding mode of oleic acid bound HSA or if instead, oleic acid bound to the nanoparticles. A negative ΔCp was observed in the interaction of HSA with copolymer particles at different temperatures which suggested that hydrophobic interactions were the driving force supported by the fact that HSA is a hydrophobic protein. However, because the observed interaction was exothermic, the authors were more inclined to think that more specific interactions may occur between the side groups of the nanoparticles and HSA. ITC was also used to study the interaction of 16 nm diameter quantum dots (functionalized using hydrophilic polymers) with proteins HSA and α-lactalbumin. An exothermic interaction was observed with HSA and a biphasic interaction was observed with α-lactalbumin (Fig. 3.18). Here ITC showed its ability to measure processes with positive ΔH of interaction (Lindman et al. 2007).

Another emerging application of nanoparticles in biomedicine is in vaccine development for example in cancer immunotherapy (Cho et al. 2011). Nanoparticles with high surface area can be used as efficient carriers to deliver target

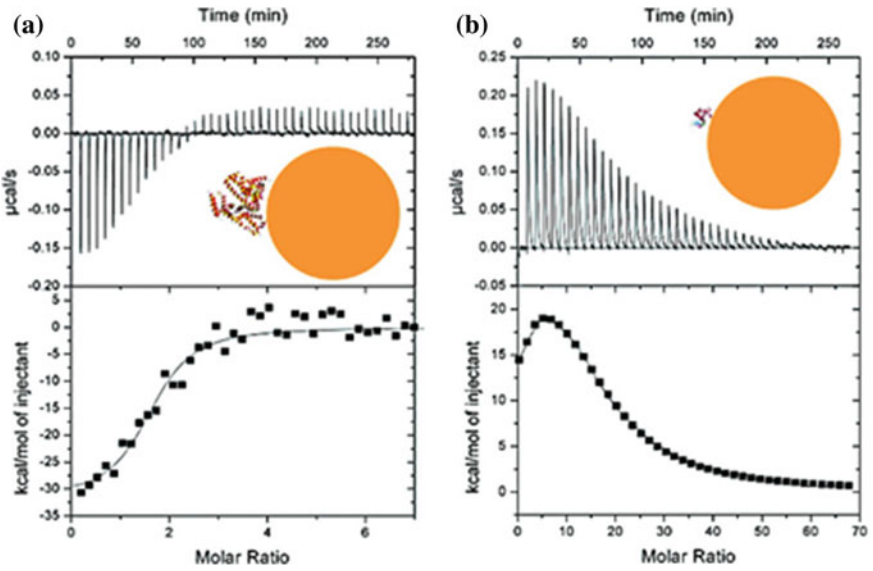

Fig. 3.18 ITC profiles showing the interaction of **a** HSA (38 μM) with a solution of 800 nm quantum dots and **b** α-lactalbumin (230 μM) with solutions of 500 nm quantum dots in Hepes/NaOH, 0.15 M NaCl, 1 mM EDTA, pH 7.5, 25 °C. *Inset* the size comparisons of the proteins and nanoparticles are illustrated. Reprinted with permission from Lindman et al. (2007) American Chemical Society

antigens to dendritic cells (DC). These cells can migrate to lymph nodes to activate T-cells specific to the antigens thereby stimulating and regulating tumor antigenic responses (Cho et al. 2011). Imaging methods such as magnetic resonance imaging (MRI) are used to track DC migration. High resolution imaging in MRI requires the use of superparamagnetic iron oxide (SPIO) nanoparticles that are not biocompatible. By coating SPIO nanoparticles with a ZnO shell that is photonic for DC-based immunotherapy, biocompatibility was achieved (Cho et al. 2011). ZnO-binding peptide (ZBP) RPHPKGGDA bound to the ZnO surface served as carriers for tumor antigens into DCs. In the peptide sequence, RPHPK is the conserved binding motif while GGDA is the linker. ITC was used to determine the binding affinity of the ZBP and a triplicate tandem repeat of it (3 × ZBP) to the ZnO coated nanoparticle (Fig. 3.19). The affinity of 3 × ZBP for the nanoparticles was higher than that of 1× ZBP (Table 3.8). The authors deduced that the high affinity of 3 × ZBP peptide for the nanoparticle surface, may suggest that zinc ions are present on the surface of the nanoparticles (Cho et al. 2011). This immunotherapy approach was tested in vivo by immunizing mice and the results were promising (Cho et al. 2011).

ITC has equally proven to be useful in industrial advancements. An example is an investigation where ITC was used to probe metal–ligand interactions in the study of interactions between divalent copper cations and chitin fragments

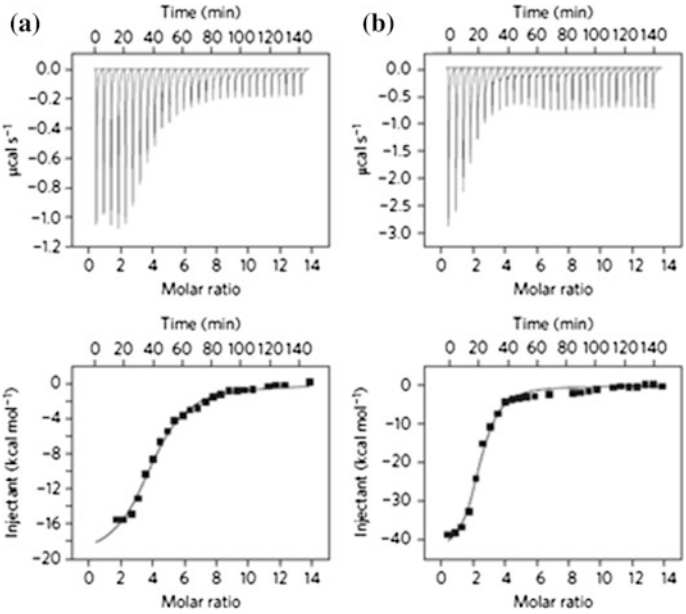

Fig. 3.19 ITC isotherms showing the interaction of 0.25 mM of **a** 1 × ZBP and **b** 3 × ZBP with a 4 μM nanoparticle suspension of ZnO coated SPIO nanoparticles at 25 °C. Reprinted by permission from Macmillan Publishers Ltd: Nature Nanotechnology (Cho et al. 2011) Nature Publishing Group

Table 3.8 Thermodynamic parameters for the interaction of ZnO-binding peptides and ZnO coated SPIO nanoparticles determined using ITC

	$K_\alpha(M^{-1})$	$K_d(M)$	ΔH° (kcal/mol)	ΔS° (kcal/mol)
I × ZBP	$6.9 \pm 0.8 \times 10^5$	1.5×10^{-6}	$-2.0 \times 10^4 \pm 757.7$	−39.9
3 × ZBP	$1.4 \pm 0.2 \times 10^6$	6.9×10^{-7}	$-4.4 \times 10^4 \pm 1208.0$	−119.0

Reprinted by permission from Macmillan Publishers Ltd: Nature Nanotechnology (Cho et al. 2011) Nature Publishing Group

(Camci-Unal and Pohl 2010). Chitin is a nontoxic, naturally abundant insoluble and inexpensive polysaccharide that can be used for biosorption of heavy metal cations found in industrial water and as a biomaterial for medical applications (Kratochvil and Volesky 1998). In previous studies, the interaction of polymeric chitin with a number of metal cations was determined to be enthalpically driven and spontaneous (Camci-Unal and Pohl 2010). The authors carried out further investigations to determine if chitin possessed specific binding sites through which multiple ligands are able to chelate a metal cation. Interaction of copper with small fragments of chitin; N-acetyl-D-glucosamine (GlcNAc), its repeating units of different lengths $(GlcNAc)_2$ $(GlcNAc)_3$ $(GlcNAc)_5$ and D-glucosamine were studied using ITC to determine if the different segments would interact with different affinities

(Camci-Unal and Pohl 2010). Once more, the values of ΔH, ΔS, and ΔG were found to be negative and they established that the interactions were enthalpically driven and spontaneous (Camci-Unal and Pohl 2010). The strength of the interaction determined from binding affinity values increased with an increase in GlcNAc residues. The deacylated GlcNAc fragment, D-glucosamine, had a higher enthalpy value and greater affinity for copper compared to GlcNAc; therefore, the authors established that the amine group is important for the interaction. The occurrence of chelation-based multivalency was ruled out because addition of sugars to the polymer did not have a drastic effect on the binding affinity beyond statistical effects; therefore, a single copper atom was not bound by multiple amide groups. The authors concluded that the findings gave information that is useful to direct computational modeling for the design of metal- and carbohydrate-based materials (Camci-Unal and Pohl 2010).

In a similar study ITC was used to compare the thermodynamic interactions between toxic metals ions (Al^{3+}, Cr^{3+}, and Pb^{2+}) with activated carbon which is a high-cost sorbent commonly used for metal decontamination of water and the same metal ions with chitin which is a possible cheaper substitute of activated carbon (Karlsen et al. 2010). The integrated heat change in kcal/mol of injectant was plotted against the amount of metal ions used (μmol) per gram of adsorbent chitin (Fig. 3.20). They then proceeded to fit data using the single set of identical sites or two sets of independent sites model to obtain thermodynamic parameters (Table 3.9). From the results, the authors deduced that there were two binding sites for the metal ions on chitin and the differences in thermodynamic signatures observed between the metal ions and chitin suggested that the metal ions may possibly bind to different functional groups found on chitin. High-cost activated carbon which is currently more commonly used to purify industrial waste water was seen to interact weakly with the metal ions at a single binding site (Karlsen et al. 2010). With this evidence, consumers can make an informed decision and may be encouraged to change from conventional use of high-cost activated carbon to low-cost chitin.

3.6 Summary, Recommendations, and Conclusions

In this chapter, we focused on the presentation of three different methods that can be used to experimentally determine thermodynamic properties that characterize the adsorption behavior of small peptides and proteins with material surfaces: SPR, AFM, and ITC. Each of these methods has its own specific set of advantages, disadvantages, and appropriate areas of application. In the preceding sections on each of these topics, we have sought to clearly identify these issues in order to provide direction for readers who may be interesting in applying these methods in their own studies to characterize peptide and protein interactions with material surfaces.

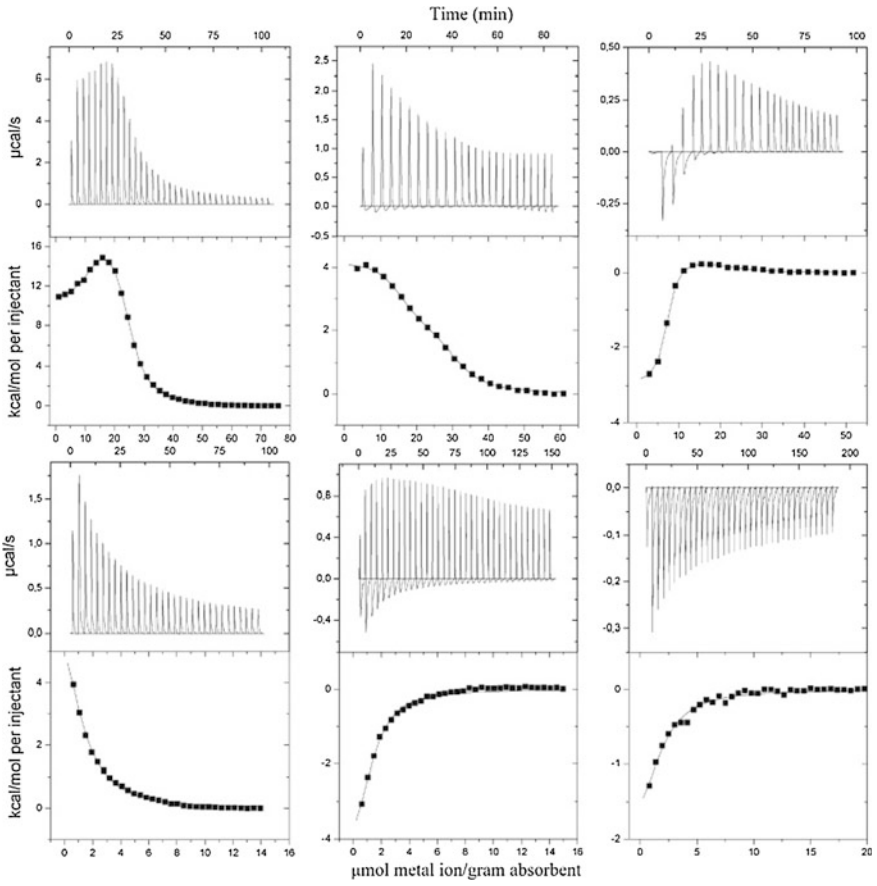

Fig. 3.20 ITC isotherms showing the interaction of metal ions Al^{3+}, Cr^{3+}, and Pb^{2+} (from *left* to *right*) with *β*-chitin (*top three*) and activated carbon (*bottom three*). Reprinted with permission from Karlsen et al. (2010) Elsevier

As a critical issue for any serious research project involving peptide/protein adsorption behavior, careful attention must be applied to ensure that the adsorbent surfaces are as clean and free from contamination as possible. Characterization methods should then be applied to document the chemical and physical properties of the adsorbent surface (e.g., chemical composition, surface energy, and surface roughness). These steps are important not only to ensure the quality of subsequent experimental results, but also so that others who wish to reproduce the results from a given study are able to closely match the conditions of the prior experiments.

As presented in Sect. 3.4, SPR spectroscopy can be used to determine the free energy of peptide adsorption to surfaces through the generation of adsorption isotherms and the application of the Langmuir model. It is important for readers to understand that the implementation of the Langmuir model is based on a set of

Table 3.9 Thermodynamic parameters for the interaction of Al^{3+}, Cr^{3+}, and Pb^{2+} with β-chitin and activated carbon at 25 °C determined using ITC

Metal ion	K_a (M^{-1})	ΔG(kJ/mol)	ΔH (kJ/mol)	ΔS (J/Kmol)	n (μ mol/g)
β-Chitin					
Al^{3*}	$(4.0 \pm 2.4) \times 10^6$	−37.6	17.6 ± 3.6	184	18
	$(2.3 \pm 0.5) \times 10^5$	−30.5	75.3 ± 5.0	355	20
Cr^{3+}	$(6.0 \pm 1.4) \times 10^6$	−38.5	16.3 ± 2.9	184	28
	$(3.6 \pm 2.8) \times 10^5$	−31.8	8.2 ± 2.1	134	31
Pb^{2+}	$(2{,}0 \pm 1.4) \times 10^7$	−41.8	−10.9 ± 1.5	105	7
	$(2.0 \pm 0.7) \times 10^5$	−30.1	2.1 ± 0.9	109	31
Activated carbon					
Al^{3*}	$(5.0 \pm 0.9) \times 10^4$	−26.8	38.5 ± 3.4	217	2
Cr^{3*}	$(6.5 \pm 1.5) \times l0^4$	−27.6	−24.3 ± 3.2	12	3
Pb^{2*}	$(4/4 \pm 1.2) \times 10^4$	−26.3	−14.2 ± 22	42	2

Reprinted with permission from Karlsen et al. (2010) Elsevier

specific conditions that must be present in order for the model to be used for the accurate determination of adsorption free energy. These conditions are that (i) the adsorption process must be fully reversible within the timeframe of the adsorption study (i.e., equilibrated conditions reached) (ii) all adsorption sites on the surface should be identical and bind only one solute molecule (i.e., homogeneous surface), (iii) solute–solute interactions do not influence the adsorption process, and (iv) the solute must adsorb as a monolayer without multilayer formation (Langmuir 1916; Everett 1964; Lan et al. 2001). Unfortunately, adsorption systems that strongly deviate from these conditions will often generate Langmuir-looking isotherms and it is therefore up to the individual user to determine that conditions i–iv are met for the adsorption process under consideration before the Langmuir model is applied. The adsorption behavior of small peptides (i.e., less than about 12 amino acid residues) onto a homogeneous material surface generally tends to follow these conditions with the exception of the influence of solute–solute interactions on the surface, which can substantially influence the amount of peptide that a surface will adsorb at saturation. The methods that we present in Sect. 3.4 enable this problem to be avoided through the use of a modified isotherm analysis approach that enables the adsorption behavior to be extrapolated to zero surface coverage, under which solute–solute interactions on the surface are minimized. The application of this analysis technique can thus provide an approach for the determination of standard-state adsorption free energy even for a system that exhibits solute–solute interactions that tend to influence the shape of the adsorption isotherm as surface saturation is approached.

One of the primary limitations of the SPR method is that the adsorbent surface must be synthesized as a thin film (i.e., <100 nm) over a metallic substrate (e.g., gold). Thus, materials that are not easily fabricated into such nano-thick layers are not amenable for use with SPR. To address this limitation, we have

developed a complementary AFM method that can be used in place of SPR. This combined set of methods is based on our findings that the force required to desorb simple unstructured peptides from a surface, as measured by a standardized AFM method, can be directly correlated to adsorption free energy measured by SPR. The critical aspect of this dual approach is the development of a correlation plot between these two methods through the use of a large set of peptide–surface systems that can be evaluated by both methods. Once this correlation plot is generated, then the same AFM protocol can be applied to measure peptide desorption forces for surfaces that are not amenable for use with SPR, with the correlation plot then used to provide estimates of adsorption free energies.

When used as a combined set, the presented SPR and AFM methods provide experimental methods that can be used to determine the change in standard-state free energy for peptide adsorption on any macroscopically flat surface. These methods, however, are not applicable to characterize the adsorption behavior of peptides with small particles that are suspended in solution. As addressed in Sect. 3.5, ITC provides an excellent experimental method to characterize these types of adsorption processes.

From the discussed case studies and other studies reported in the literature it is clear that ITC is an invaluable tool for thermodynamic characterization of interfacial interactions with small particles. ITC has developed from its conventional use to study equilibrium processes to a universal tool that can be used to investigate irreversible processes of binding/adsorption of artificial molecules and biopolymers on surfaces or with each other (Chiad et al. 2009; Schmidtchen 2012).

Like any other technique, ITC has limitations and challenges that need to be recognized. From the studies we have discussed we can already begin to understand some of these challenges. The importance of sample preparation and characterization especially of particles before carrying out ITC studies has been underlined. In an experiment, the user seeks to achieve a measurable heat change under optimum conditions to obtain a profile from which thermodynamic parameters can accurately be obtained. As thermodynamic parameters are calculated from concentrations, integrated heat change should be plotted against the molar ratio of interacting species for thermodynamic parameters to be determined. For interactions of peptides with surfaces, we agree with the proposed method to express the binding site for a ligand (i.e., protein) on a surface (i.e., inorganic particles) as the effective concentration of sites on the surface available for interaction so that data can be plotted as normalized integrated heat change in kcal/mole of injectant against the molar ratio of reactants ([protein]/[inorganic surface sites]) (Goobes R et al. 2007) even though this information may be difficult to obtain in practice especially where multilayers of protein are adsorbed without a clear distinction between the saturation of the protein-surface and protein–protein adsorption event. The shapes of isothermal profiles from different interactions can vary dramatically and modeling of ITC data can become challenging especially if there are multiple binding sites involved and where there is no knowledge on

whether the sites are dependent or independent. Prior knowledge about the binding site of the interaction gives a clearer view as to which fitting model should be used. However, in many cases when studying interactions of molecules with inorganic particles, the exact binding site can be difficult to define (Ball and Maechline 2009). On detailed inspection of literature, one can begin to appreciate that there are uncertainties in using mathematical models when it comes to appropriate representation of an interaction being studied. In some studies, when unsure, authors have decided to fit data using more than one binding model and in many cases it is not clear why authors chose to use a particular model especially when there is no strong relation to the interaction being studied. Meaningful representation of data should be pursued. An expert in the use of ITC has even said that "All models are wrong, but some are useful" (Freyer and Lewis 2008). Mathematical expertise is valuable for developing additional useful models besides those provided in commercial software. Nonetheless using the simplest models with the fewest adjustable parameters are recommended (Schmidtchen 2012).

Data interpretation and deconvolution of individual events (i.e., van der Waals interactions, electrostatic interactions, hydrogen bonding, and hydrophobic interactions) occurring simultaneously and contributing to the global heat change is not always straightforward and cannot be described at the atomic level. Improvements in technology and methodology are needed especially where ITC experiments have to be simplified compared to the actual events they need to be correlated to (Cliff et al. 2004; Mahmoudi et al. 2011). For example in drug development it may only be possible to study interactions of individual proteins with nanoparticles using ITC to obtain information that can be assertively interpreted; however, in biological fluids, we know that there are several proteins of different affinities in coexistence and that cooperative effects must play an important role (Cliff et al. 2004; Mahmoudi et al. 2011). Complementary techniques are useful especially where more than one interaction occurs simultaneously and where interactions occur producing heat changes that are below the detection limit of the instrument (Goobes R et al. 2007; Lindman et al. 2007). Great prospects lie in using information obtained from ITC studies to advance design processes thereby creating novel materials. With continued improvements in instrumentation and methodology, the development of novel applications of ITC is far from being exhausted.

Acknowledgments R.A. Latour and Y. Wei would like to acknowledge support for this research from the Defense Threat Reduction Agency-Joint Science and Technology Office for Chemical and Biological Defense (Grant no. HDTRA1-10-1-0028). The facilities used were also supported by NIH Grants 5P20RR021949-04 and 8P20GM103444-04. We also would like to thank Ms. Megan Grobman, Dr. Lara Gamble, and Dr. David Castner of NESAC/BIO at the University of Washington for assistance with surface characterization with XPS under the funding support by NIH NIBIB (grant # EB002027). C.C. Perry and M.J. Limo would like to thank their collaborators at the Air force office of scientific research (AFOSR) for funding and support of their studies (FA9550-10-1-0024 and FA9550-13-1-0040).

References

Ababou A, Ladbury JE (2006) Survey of the year 2004: literature on applications of isothermal titration calorimetry. J Mol Recogn 19(1):79–89

Allison DP, Hinterdorfer P, Han W (2002) Biomolecular force measurements and the atomic force microscope. Curr Opin Biotechnol 13(1):47–51

Ball V, Maechling C (2009) Isothermal microcalorimetry to investigate non specific interactions in biophysical chemistry. Int J Mol Sci 10(8):3283–3315

Biltonen R, Langerman N (1979) Microcalorimetry for biological chemistry: experimental design, data analysis, and interpretation. Methods Enzymol 61:287–318

Blanchette CD, Loui A, Ratto TV (2008) Tip functionalization: applications to chemical force spectroscopy. Handbook of Molecular Force Spectroscopy, pp 185–203

Blankschien MD, Pretzer LA, Huschka R et al (2013) Light-triggered biocatalysis using thermophilic enzyme-gold nanoparticle complexes. ACS Nano 7(1):654–663

Bouchemal K, Mazzaferro S (2012) How to conduct and interpret ITC experiments accurately for cyclodextrin-guest interactions. Drug Discov Today 17(11):623–629

Bramwell VW, Eyles JE, Oya Alpar H (2005) Particulate delivery systems for biodefense subunit vaccines. Adv Drug Deliv Rev 57:1247–1265

Bryers JD, Giachelli CM, Ratner BD (2012) Engineering biomaterials to integrate and heal: the biocompatibility paradigm shifts. Biotechnol Bioeng 109(8):1898–1911

Camci-Unal G, Pohl NLB (2010) Thermodynamics of binding interactions between divalent copper and chitin fragments by isothermal titration calorimetry (ITC). Carbohydr Polym 81(1):8–13

Cedervall T, Lynch I, Lindman S, Berggard et al (2007) Understanding the nanoparticle-protein corona using methods to quantify exchange rates and affinities of proteins for nanoparticles. Proc Natl Acad Sci USA 104(7):2050–2055

Charles MR, Abraham ML (2003) Quanatitative modeling of protein adsorption. Biopolymers at Interfaces. M. M. Dekker, New York, pp 71–94

Chen Y, Ming H (2012) Review of surface plasmon resonance and localized surface plasmon resonance sensor. Photonic Sens 2(1):37–49

Chen K, Xu Y, Rana S et al (2011) Electrostatic selectivity in protein–nanoparticle interactions. Biomacromolecules 12(7):2552–2561

Chiad K, Stelzig SH, Gropeanu R et al (2009) Isothermal titration calorimetry: a powerful technique to quantify interactions in polymer hybrid systems. Macromolecules 42(19):7545–7552

Chilom CG, Craescu CT, Popescu AI (2004) Parameters of interaction between proteins and their specific ligands, deduced by isothermal titration calorimetry. In: Paper presented at the 5th International Balkan workshop on applied physics, pp 443–457

Chiu CY, Li Y, Ruan L et al (2011) Platinum nanocrystals selectively shaped using facet-specific peptide sequences. Nat Chem 3(5):393–399

Cho N, Cheong T, Min JH et al (2011) A multifunctional core-shell nanoparticle for dendritic cell-based cancer immunotherapy. Nat Nanotechnol 6(10):675–682

Cliff MJ, Gutierrez A, Ladbury JE (2004) A survey of the year 2003 literature on applications of isothermal titration calorimetry. J Mol Recogn 17(6):513–523

Crespo-Quesada M, Andanson J, Yarulin A et al (2011) UV–ozone cleaning of supported poly (vinylpyrrolidone)-stabilized palladium nanocubes: effect of stabilizer removal on morphology and catalytic behavior. Langmuir 27(12):7909–7916

Davis SA, Dujardin E, Mann S (2003) Biomolecular inorganic materials chemistry. Curr Opin Solid State Mater Sci 7(4–5):273–281

de Mol NJ, Fischer MJ (2010) Surface plasmon resonance: a general introduction. Methods Mol Biol 627:1–14

De M, You C, Srivastava S et al (2007) Biomimetic interactions of proteins with functionalized nanoparticles: a thermodynamic study. J Am Chem Soc 129(35):10747–10753

Dickerson MB, Sandhage KH, Naik RR (2008) Protein-and peptide-directed syntheses of inorganic materials. Chem Rev 108(11):4935–4978

Dujardin E, Mann S (2002) Bio-inspired materials chemistry. Adv Mater 14(11):775

Everett DH (1964) Thermodynamics of adsorption from solution. Part 1. Perfect systems. Trans Faraday Soc 60:1803–1813

Fears KP, Creager SE, Latour RA (2008) Determination of the surface pK of carboxylic- and amine-terminated alkanethiols using surface plasmon resonance spectroscopy. Langmuir 24(3):837–843

Fenoglio I, Fubini B, Ghibaudi EM et al (2011) Multiple aspects of the interaction of biomacromolecules with inorganic surfaces. Adv Drug Deliv Rev 63(13):1186–1209

Freyer MW, Lewis EA (2008) Isothermal titration calorimetry: experimental design, data analysis, and probing macromolecule/ligand binding and kinetic interactions. Methods Cell Biol 84:79–113

Gandavarapu NR, Mariner PD, Schwartz MP et al (2013) Extracellular matrix protein adsorption to phosphate-functionalized gels from serum promotes osteogenic differentiation of human mesenchymal stem cells. Acta Biomater 9(1):4525–4534

Garcia AJ (2006) Interfaces to control cell-biomaterial adhesive interactions. Polymers for Regenerative Medicine. C. Werner, J. H. Eisseeff, C. Fischbachet al:171–190

Geelhood SJ, Horbett TA, Ward WK et al (2007) Passivating protein coatings for implantable glucose sensors: evaluation of protein retention. J Biomed Mater Res B 81B(1):251–260

Goobes G, Goobes R, Shaw WJ et al (2007) The structure, dynamics, and energetics of protein adsorption—lessons learned from adsorption of statherin to hydroxyapatite. Magn Reson Chem 45(S1):S32–S47

Goobes R, Goobes G, Shaw WJ et al (2007) Thermodynamic roles of basic amino acids in statherin recognition of hydroxyapatite. Biochemistry 46(16):4725–4733

Gourishankar A, Shukla S, Ganesh KN et al (2004) Isothermal titration calorimetry studies on the binding of DNA bases and PNA base monomers to gold nanoparticles. J Am Chem Soc 126(41):13186–13187

Green RJ, Frazier RA, Shakesheff KM et al (2000) Surface plasmon resonance analysis of dynamic biological interactions with biomaterials. Biomaterials 21(18):1823–1835

Gref R, Domb A, Quellec P et al (2012) The controlled intravenous delivery of drugs using PEG-coated sterically stabilized nanospheres. Adv Drug Deliv Rev 64:316–326

Haruki M, Noguchi E, Kanaya S et al (1997) Kinetic and stoichiometric analysis for the binding of Escherichia coli ribonuclease HI to RNA–DNA hybrids using surface plasmon resonance. J Biol Chem 272(35):22015–22022

Herr AE (2009). Protein microarrays for the dectection of biothreats. In: Dill RHLK, Grodzinski P (eds) Microarrays. Preparation, microfluidics, detection methods, and biological applications. Springer, New York, pp 169–190

Hoffmann F, Cornelius M, Morell J et al (2006) Silica-based mesoporous organic–inorganic hybrid materials. Angew Chem Int Ed 45(20):3216–3251

Homola J, Yee SS, Gauglitz G (1999) Surface plasmon resonance sensors: review. Sens Actuators B Cheml 54(1–2):3–15

Horinek D, Serr A, Geisler M et al (2008) Peptide adsorption on a hydrophobic surface results from an interplay of solvation, surface, and intrapeptide forces. Proc Natl Acad Sci U S A 105(8):2842–2847

Huang R, Carney R, Stellacci F et al (2013) Protein-nanoparticle interactions: the effects of surface compositional and structural heterogeneity is scale dependent. Nanoscale 5:6928–6935

Jana NR, Gearheart L, Murphy CJ (2001) Seeding growth for size control of 5–40 nm diameter gold nanoparticles. Langmuir 17(22):6782–6786

Jiang X, Ortiz C, Hammond PT (2002) Exploring the rules for selective deposition: Interactions of model polyamines on acid and oligoethylene oxide surfaces. Langmuir 18(4):1131–1143

Joshi H, Shirude PS, Bansal V et al (2004) Isothermal titration calorimetry studies on the binding of amino acids to gold nanoparticles. J Phys Chem B 108(31):11535–11540

Jung LS, Nelson KE, Campbell CT et al (1999) Surface plasmon resonance measurement of binding and dissociation of wild-type and mutant streptavidin on mixed biotin-containing alkylthiolate monolayers. Sens Actuators B Chem 54(1–2):137

Karlsen V, Heggset EB, Sørlie M (2010) The use of isothermal titration calorimetry to determine the thermodynamics of metal ion binding to low-cost sorbents. Thermochim Acta 501(1–2):119–121

Kasemo B, Gold J (1999) Implant surfaces and interface processes. Adv Dent Res 13:8–20

Kidoaki S, Matsuda T (2002) Mechanistic aspects of protein/material interactions probed by atomic force microscopy. Colloids Surf B 23(2–3):153–163

Klein J (2007) Probing the interactions of proteins and nanoparticles. Proc Natl Acad Sci 104(7):2029–2030

Knowles JR (1991) Enzyme catalysis: not different, just better. Nature 350:121–124

Kratochvil D, Volesky B (1998) Advances in the biosorption of heavy metals. Trends Biotechnol 16(7):291–300

Kröger N, Deutzmann R, Sumper M (1999) Polycationic peptides from diatom biosilica that direct silica nanosphere formation. Science 286(5442):1129–1132

Kumar A, Mandal S, Pasricha R et al (2003) Investigation into the interaction between surface bound alkylamines and gold nanoparticles. Langmuir 19(15):6277–6282

Ladbury JE, Doyle ML (2005) Biocalorimetry 2: applications of calorimetry in the biological sciences. Wiley, Chichester

Lal R, John SA (1994) Biological applications of atomic force microscopy. Am J Physiol Cell Physiol 266(1):C1–C21

Lan Q, Bassi AS, Zhu J-X et al (2001) A modified Langmuir model for the prediction of the effects of ionic strength on the equilibrium characteristics of protein adsorption onto ion exchange/affinity adsorbents. Chem Eng J 81:179–186

Langmuir I (1916) The constitution and fundamental properties of solids and liquids. part i. solids. J Am Chem Soc 38:2221–2295

Latour RA (2008) Molecular dynamics simulation of protein-surface interactions: benefits, problems, solutions, and future directions. Biointerphases 3:FC2–FC12

Leavitt S, Freire E (2001) Direct measurement of protein binding energetics by isothermal titration calorimetry. Curr Opin Struct Biol 11(5):560–566

Li X, Husson SM (2006) Adsorption of dansylated amino acids on molecularly imprinted surfaces: a surface plasmon resonance study. Biosens Bioelectron 22(3):336–348

Liang Y (2008) Applications of isothermal titration calorimetry in protein science. Acta Biochim Biophys Sin 40(7):565–576

Liang M, Deschaume O, Patwardhan SV et al (2011) Direct evidence of ZnO morphology modification via the selective adsorption of ZnO-binding peptides. J Mater Chem 21(1):80–89

Lindman S, Lynch I, Thulin E et al (2007) Systematic investigation of the thermodynamics of HSA adsorption to N-iso-propylacrylamide/N-tert-butylacrylamide copolymer nanoparticles. Effects of particle size and hydrophobicity. Nano Lett 7(4):914–920

Liu HN, Webster TJ (2010) Ceramic/polymer nanocomposites with tunable drug delivery capability at specific disease sites. J Biomed Mater Res A 93A(3):1180–1192

Loomans E, Beumer TAM, Damen KCS et al (1997) Real-time monitoring of peptide-surface and peptide-antibody interaction by means of reflectometry and surface plasmon resonance. J Colloid Interface Sci 192(1):238–249

Lynch I, Dawson KA (2008) Protein-nanoparticle interactions. Nano Today 3(1):40–47

Mahmood TA, Miot S, Frank O et al (2006) Modulation of chondrocyte phenotype for tissue engineering by designing the biologic-polymer carrier interface. Biomacromolecules 7(11):3012–3018

Mahmoudi M, Lynch I, Ejtehadi MR et al (2011) Protein-nanoparticle interactions: opportunities and challenges. Chem Rev 111(9):5610–5637

Martinez JC, Murciano-Calles J, Cobos ES et al (2013) Isothermal titration calorimetry: thermodynamic analysis of the binding thermograms of molecular recognition events by using equilibrium models. In: Elkordy AA (ed) Chapter 4, Applications of Calorimetry in a Wide

Context-Differential Scanning Calorimetry, Isothermal Titration Calorimetry and Microcalorimetry. InTech—Open Access Company, pp 73–104
Mazaheri M, Zahedi AM, Sadrnezhaad SK (2008) Two-step sintering of nanocrystalline ZnO compacts: effect of temperature on densification and grain growth. J Am Ceram Soc 91(1):56–63
MicroCal L (2003) VP–ITC microcalorimeter user's manual. Microcal, Llc pp 1–94
Monzó J, Koper M, Rodriguez P (2012) Removing polyvinylpyrrolidone from catalytic Pt nanoparticles without modification of superficial order. ChemPhysChem 13(3):709–715
Naik RR, Brott LL, Clarson SJ et al (2002) Silica-precipitating peptides isolated from a combinatorial phage display peptide library. J Nanosci Nanotechnol 2(1):95–100
Oka K, Shibata H, Kashiwaya S (2002) Crystal growth of ZnO. J Cryst Growth 237–239, Part 1:509–513
Oren EE, Tamerler C, Sarikaya M (2005) Metal recognition of septapeptides via polypod molecular architecture. Nano Lett 5(3):415–419
Perozzo R, Folkers G, Scapozza L (2004) Thermodynamics of protein-ligand interactions: history, presence, and future aspects. J Recept Signal Transduct 24(1–2):1–52
Perry CC, Patwardhan SV, Deschaume O (2009) From biominerals to biomaterials: the role of biomolecule-mineral interactions. Biochem Soc Trans 37:687–691
Pierce MM, Raman C, Nall BT (1999) Isothermal titration calorimetry of protein–protein interactions. Methods 19(2):213–221
Pirzer T, Geisler M, Scheibel T et al (2009) Single molecule force measurements delineate salt, pH and surface effects on biopolymer adhesion. Phys Biol 6(2):25004
Pitarke JM, Silkin VM, Chulkov EV et al (2007) Theory of surface plasmons and surface-plasmon polaritons. Rep Prog Phys 70(1):1
Poon GM (2010) Explicit formulation of titration models for isothermal titration calorimetry. Anal Biochem 400(2):229–236
Raj P, Johnsson M, Levine MJ et al (1992) Salivary statherin. dependence on sequence, charge, hydrogen bonding potency, and helical conformation for adsorption to hydroxyapatite and inhibition of mineralization. J Biol Chem 267(9):5968–5976
Rautaray D, Mandal S, Sastry M (2005) Synthesis of hydroxyapatite crystals using amino acid-capped gold nanoparticles as a scaffold. Langmuir 21(11):5185–5191
Rezwan K, Studart A, Vörös J et al (2005) Change of ζ potential of biocompatible colloidal oxide particles upon adsorption of bovine serum albumin and lysozyme. J Phys Chem B 109(30):14469–14474
Rioux R, Song H, Grass M et al (2006) Monodisperse platinum nanoparticles of well-defined shape: synthesis, characterization, catalytic properties and future prospects. Top Catal 39(3):167–174
Ruan L, Ramezani-Dakhel H, Chiu C et al (2013) Tailoring molecular specificity toward a crystal facet: a lesson from biorecognition toward Pt {111}. Nano Lett 13(2):840–846
Sabia R, Ukrainczyk L (2000) Surface chemistry of SiO_2 and TiO_2–SiO_2 glasses as determined by titration of soot particles. J Non-Cryst Solids 277(1):1–9
Sanford K, Kumar M (2005) New proteins in a materials world. Curr Opin Biotechnol 16(4):416–421
Sarikaya M, Tamerler C, Jen AKY et al (2003) Molecular biomimetics: nanotechnology through biology. Nat Mater 2(9):577–585
Schmidtchen, F.P. (2012) Isothermal titration calorimetry in supramolecular chemistry. Supramolecular Chemistry: From Molecules to Nanomaterials, 67-103
Sigurskjold BW (2000) Exact analysis of competition ligand binding by displacement isothermal titration calorimetry. Anal Biochem 277(2):260–266
Silin VV, Weetall H, Vanderah DJ (1997) SPR studies of the nonspecific adsorption kinetics of human IgG and BSA on gold surfaces modified by self-assembled monolayers (SAMs). J Colloid Interface Sci 185(1):94–103

Snyder JA, Abramyan T, Yancey JA et al (2012) Development of a tuned interfacial force field parameter set for the simulation of protein adsorption to silica glass. Biointerphases 7(1–4):51–12 (article 56)

Song H, Kim F, Connor S et al (2005) Pt nanocrystals: shape control and Langmuir-Blodgett monolayer formation. J Phys Chem B 109(1):188–193

Stenberg E, Persson B, Roos H et al (1991) Quantitative determination of surface concentration of protein with surface plasmon resonance using radiolabeled proteins. J Colloid Interface Sci 143(2):513–526

Tamerler C, Oren EE, Duman M et al (2006) Adsorption kinetics of an engineered gold binding Peptide by surface plasmon resonance spectroscopy and a quartz crystal microbalance. Langmuir 22(18):7712–7718

Taylor AD, Ladd J, Homola J et al (2008) Surface plasmon resonance (SPR) sensors for the detection of bacterial pathogens. In: Zourob M, Elwary S, Turner A (eds) Principles of bacterial detection: biosensors, recognition receptors and microsystems, Springer, New York, pp 83–108

Thomson JA, Ladbury JE (2004) Isothermal titration calorimetry: a tutorial. Biocalorimetry 2:37–58

Thyparambil AA, Wei Y, Latour RA (2012) Determination of peptide-surface adsorption free energy for material surfaces not conducive to SPR or QCM using AFM. Langmuir 28(13):5687–5694

Togashi T, Yokoo N, Umetsu M et al (2011) Material-binding peptide application—ZnO crystal structure control by means of a ZnO-binding peptide. J Biosci Bioeng 111(2):140–145

Tomczak M, Gupta MK, Drummy LF et al (2009) Morphological control and assembly of zinc oxide using a biotemplate. Acta Biomater 5(3):876–882

Velazquez-Campoy A, Kiso Y, Freire E (2001) The binding energetics of first-and second-generation HIV-1 protease inhibitors: implications for drug design. Arch Biochem Biophys 390(2):169–175

Vellore NA, Yancey JA, Collier G et al (2010) Assessment of the transferability of a protein force field for the simulation of peptide-surface interactions. Langmuir 26:7396–7404

Vernekar VN, Latour RA (2005) Adsorption thermodynamics of a mid-chain peptide residue on functionalized SAM surfaces using SPR. Mater Res Innov 9:337–353

Wei Y, Latour RA (2008) Determination of the adsorption free energy for peptide-surface interactions by SPR spectroscopy. Langmuir 24(13):6721–6729

Wei Y, Latour RA (2009) Benchmark experimental data set and assessment of adsorption free energy for peptide-surface interactions. Langmuir 25(10):5637–5646

Wei Y, Latour RA (2010) Correlation between desorption force measured by atomic force microscopy and adsorption free energy measured by surface plasmon resonance spectroscopy for peptide-surface interactions. Langmuir 26(24):18852–18861

Wei Y, Thyparambil AA, Latour RA (2012) Peptide–surface adsorption free energy comparing solution conditions ranging from low to medium salt concentrations. ChemPhysChem 13(17):3782–3785

Whyburn GP, Li YJ, Huang Y (2008) Protein and protein assembly based material structures. J Mater Chem 18(32):3755–3762

Wikiel K, Burke EM, Perich JW et al (1994) Hydroxyapatite mineralization and demineralization in the presence of synthetic phosphorylated pentapeptides. Arch Oral Biol 39(8):715–721

Willemsen OH, Snel MM, Cambi A et al (2000) Biomolecular interactions measured by atomic force microscopy. Biophys J 79(6):3267–3281

Wiseman T, Williston S, Brandts JF et al (1989) Rapid measurement of binding constants and heats of binding using a new titration calorimeter. Anal Biochem 179(1):131–137

Wisniewski N, Moussy F, Reichert WM (2000) Characterization of implantable biosensor membrane biofouling. Fresenius' J Anal Chem 366(6):611

Wu H, Zhang CH, Liang YP et al (2013) Catechol modification and covalent immobilization of catalase on titania submicrospheres. J Mol Catal B-Enzym 92:44–50

You CC, Agasti SS, Rotello VM (2008) Isomeric control of protein recognition with amino acid- and dipeptide-functionalized gold nanoparticles. Chem Eur J 14(1):143–150

You C, De M, Han G, Rotello VM (2005a) Tunable inhibition and denaturation of α-chymotrypsin with amino acid-functionalized gold nanoparticles. J Am Chem Soc 127(37):12873–12881

You C, De M, Rotello VM (2005b) Contrasting effects of exterior and interior hydrophobicmoieties in the complexation of amino acid functionalized gold clusters with α-chymotrypsin. Org Lett 7(25):5685–5688

Zhang Z, Menges B, Timmons RB et al (2003) Surface plasmon resonance studies of protein binding on plasma polymerized di(ethylene glycol) monovinyl ether films. Langmuir 19(11):4765–4770